Influence of Forced Convection on Sessile Droplet Evaporation

by

Henry Fung

A thesis submitted to the
School of Graduate and Postdoctoral Studies in partial
fulfillment of the requirements for the degree of

Masters of Applied Science in Mechanical Engineering

The Faculty of Engineering and Applied Science

University of Ontario Institute of Technology

Oshawa, Ontario, Canada

April 2019

Thesis Examination Information

Submitted by: **Henry Fung**

Master of Applied Science in **Mechanical Engineering**

Thesis title: Influence of Forced Convection on Sessile Droplet Evaporation

An oral defense of this thesis took place on April 16, 2019 in front of the following examining committee:

Examining Committee:

Chair of Examining Committee	Dr. Martin Agelin-Chaab
Research Supervisor	Dr. Brendan MacDonald
Examining Committee Member	Dr. Martin Agelin-Chaab
External Examiner	Dr. Amirkianoosh Kiani, UOIT Manufacturing Engineering Faculty

The above committee determined that the thesis is acceptable in form and content and that a satisfactory knowledge of the field covered by the thesis was demonstrated by the candidate during an oral examination. A signed copy of the Certificate of Approval is available from the School of Graduate and Postdoctoral Studies.

Abstract

Evaporation is a phase change process with potential for achieving large heat transfer rates under high air temperatures due to the latent heat of vaporization. Bioinspired artificial perspiration systems can leverage the evaporation of sessile droplets to implement this effect for different cooling applications. In the case of human perspiration, droplet evaporation typically occurs under exposure to moving air, or forced convection. However, current approaches to understanding droplet evaporation primarily use a vapour-diffusion limited model. Experiments using an open-loop wind tunnel and computer-vision based control system were conducted to measure evaporation rates of continuously-fed sessile droplets under forced convection. Results demonstrated increases to the evaporation rate with the inclusion of forced convection and removal of the vapour-diffusion limit, but also shows evidence for a limit based on thermal behavior. Additional experiments also demonstrate boundary layer effects caused by adjacent droplets suppresses increases to the evaporation rates from forced convection.

Keywords: Sessile droplet; Evaporation; Forced Convection

Author's Declaration

I hereby declare that this thesis consists of original work of which I have authored. This is a true copy of the thesis, including any required final revisions, as accepted by my examiners.

I authorize the University of Ontario Institute of Technology to lend this thesis to other institutions or individuals for the purpose of scholarly research. I further authorize University of Ontario Institute of Technology to reproduce this thesis by photocopying or by other means, in total or in part, at the request of other institutions or individuals for the purpose of scholarly research. I understand that my thesis will be made electronically available to the public.

Henry Fung

Acknowledgements

Firstly, I would like to thank my supervisor, Dr. Brendan MacDonald for his support and guidance throughout this stage of my education. Your encouragement and trust in my abilities during the most trying of times have been invaluable, and your passion for learning and the engineering profession is truly inspiring.

To my fellow colleagues and friends with whom I've shared good times and bad in MacDonald Lab: Salvatore Ranieri, Michael Crowley, Md. Almostasim Mahmud, Anders Nielsen, Justin Rizzi and William Oishi, my deep gratitude goes to all of you for your inspiration and support. The endless debates we've had about society, academics and life, often in the face of impending deadlines, are some of the most thought-provoking experiences I've ever had and will be remembered fondly. Thanks to Chirag Karia, for providing the pivotal suggestion to learn Python and providing your generous help and expertise. Thanks to my examining committee, Dr. Martin Agelin-Chaab and Dr. Brendan MacDonald for providing the time and effort to examine my work and special thanks to Dr. Amirkianoosh Kiani for agreeing to be the external examiner and providing valuable assessment.

To my wonderful better half, Katie Mak, thank you for constantly giving me unwavering love and support during my entire engineering education. You lift my spirits while keeping me balanced and grounded; you are truly instrumental to my successes.

To my mother Bun Yee Tong, I owe my greatest appreciation; without your unconditional love and unyielding perseverance, I would not be here.

Contents

List of Tables

List of Figures

Nomenclature

$\dot{m}_{evap}$	Droplet evaporation mass flow rate	kg/s
$\dot{m}_{pump}$	Pump mass flow rate	kg/s
c_0	Local vapour concentration	g/m^3
c_p	Specific heat capacity	J/kg K
c_∞	Far-field vapour concentration	g/m^3
c_v	Saturation vapour concentration	g/m^3
D	Diffusion coefficient of water into air	m^2/s
g	Acceleration due to gravity	9.8 m/s^2
H	Relative Humidity	%RH
h	Boundary layer height	m
h_e	Contraction exit height	m
h_i	Contraction inlet height	m
k	Thermal conductivity	W/m K
L	Characteristic length	m
q_{cond}	Heat conduction from the substrate	J/kg K
$q_{conv,e}$	Heat transfer from external convection outside droplet	J/kg K
$q_{conv,i}$	Heat transfer from internal convection inside droplet	J/kg K
Q_{evap}	Droplet evaporation rate	μL/min
q_{evap}	Latent heat of vaporization	J/kg K

R	Droplet radius	mm
T_a	Ambient air temperature	°C
T_s	Substrate temperature	°C
U	Air velocity	m/s
U'	Standard deviation of air velocity fluctuations	m/s
U_{avg}	Average air velocity	m/s
x	Flat plate length	m
x'	Normalized Contraction height	m
Bo	Bond number	
We	Weber number	

Greek Letters

ν	Kinematic viscosity	m^2/s
ρ	Density	kg/m^3
σ	Surface Tension	m^2/s

Chapter 1

Introduction

As the pace of technological change continues to accelerate in the 21st century, cooling and heat removal technology will remain a key aspect of future development. Anthropomorphic climate change is rapidly changing the biosphere and a major consequence of this is rising temperatures worldwide, exacerbating extreme weather events. Meanwhile, a significant portion of the human population resides within regions which will bear the worst of these effects [1]. In the coming decades, this will drive an increase in demand for innovations in HVAC technologies, particularly in cooling and thermal management due to the higher temperatures. Alongside demands related to health and comfort, rapid economic growth is driving the implementation of advanced electronics in a variety of industrial applications, exposing sensitive components to harsh conditions. In these cases, technologies such as autonomous drones and remote sensing electronics must be resilient against the hot environments they will be exposed to as well as sustain adequate heat rejection to maintain computing performance. The aforementioned examples highlight a demand for innovations in thermal management, with an emphasis on operation in high temperature conditions.

Phase-change or evaporative cooling technology holds potential for addressing these constraints where traditional approaches to heat removal are limited. Human perspiration is a prime example of this effect in nature, whereby the evaporation of sweat droplets excreted from the skin can effectively cool the body during periods of exertion or overheating, even in exposure to high ambient air temperatures. The body is also typically exposed to a moving air flow under these conditions, either by movement during exercise, or the surrounding wind/breeze. Bioinspired simulated skin systems leveraging this approach could provide significant cooling where traditional radiator and fan systems may not be adequate. Drones and specialized electronics in particular may benefit from this innovative technique due to their widespread application in a variety of environmental conditions.

In order to develop effective designs leveraging this principle, more work is required to understand the underlying heat and mass transfer mechanisms in evaporating sessile droplets. Presently, the majority of work regarding droplet evaporation is focused on diffusion limited models in quiescent environments. This thesis will investigate the influence of moving air, otherwise known as forced convection, on the evaporation rate of a single droplet.

1.1 Background

1.1.1 Sessile Droplet Parameters

The complex phenomenon of human perspiration may be roughly approximated as a case of sessile droplet evaporation. The term *sessile* is defined as *being attached at the base* and originates from the latin word *sessilis* meaning *fit for sitting*. In this context, it refers to a liquid droplet resting on top of a solid substrate, as shown in Figure 1. Liquid droplets which hang or suspend from solid surfaces are known as pendant droplets, or may be completely immersed in gas as a suspended droplet; in these configurations, the mass and energy transport mechanisms differ greatly from sessile droplets. A sessile droplet forms a finite contact area due to various material properties of the surface, such as roughness and surface energy which define

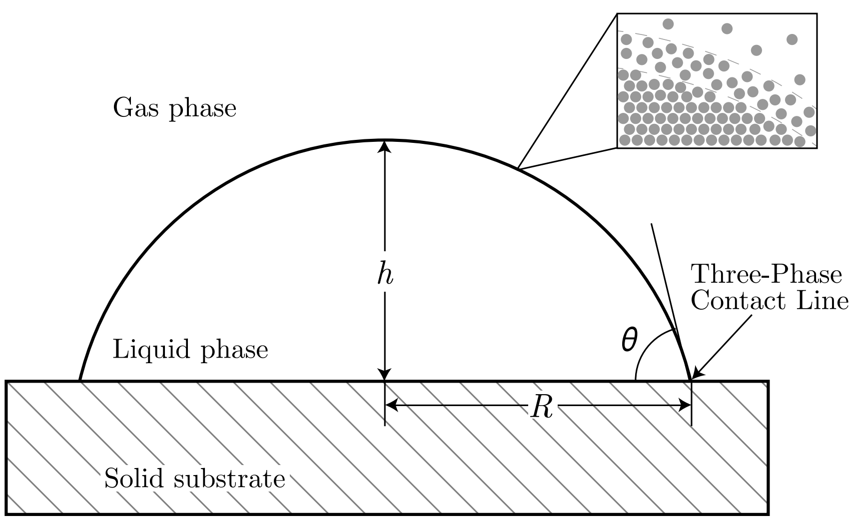

Figure 1: A sessile droplet on a flat substrate. Inset diagram shows an illustration of the interfacial region.

the wettability. For cases of large liquid volumes or a highly wettable surface, the liquid spreads to form a film rather than remain in a cohesive droplet shape, drastically changing the geometry and physical mechanisms involved. The tendency for molecules in the liquid phase to form bonds with one another results in higher energy for molecules at the surface of the liquid-gas interface [2], otherwise known as surface tension. This effect causes droplets to naturally prefer spherical geometries which minimizes the surface-area-to-volume ratio, and in sessile droplets, forms a circular contact area with a contact radius, R. This surface tension effect also gives rise to a curved liquid-vapour interface, with the apex of curvature located a height, h, from the solid substrate, and produce a contact angle, θ, at the location where solid, liquid and gas phases meet, known as the three-phase contact line.

While droplets preferentially form spherical geometries, the resulting shape may be altered by external influences, and analytically predicting the droplet shape for a given liquid volume is challenging. For small liquid volume, the droplet shape may be approximated as that of a hemisphere. The validity of this approximation is assessed using the Bond number which is the ratio of gravitational to surface tension forces,

$$Bo = \frac{\Delta\rho g L^2}{\sigma} \tag{1.1}$$

where $\Delta\rho$ is the difference in density between the liquid and gas phases, g is the acceleration due to gravity, L is characteristic length scale which corresponds to the droplet radius in this case, and σ is the surface tension of the interface. The hemisphere approximation is valid for droplets whose Bo<0.25 [3]; for a water droplet at ambient temperature and terrestrial gravity, this corresponds to a contact radius $R \approx 1.33$ mm, and a droplet volume of $\approx 5\mu$L at a contact angle of $90°$. The droplets considered in the following discussions will be approximately this size range.

1.1.2 Principles of Droplet Evaporation

Evaporation is a surface phenomenon in which a substance changes phase from liquid to vapour at the interface between the two bulk phases. Atmospheric air is a mixture of dry air and water vapour; the ratio of water vapour to dry air is commonly known as relative humidity (%RH). Atmospheric pressure may be viewed as the sum of partial pressures of air and water vapour; the partial pressure of water vapour is also known as the vapour pressure. Evaporation occurs as a result of the vapour pressure being less than the saturation pressure of water vapour in air [4]. When atmospheric pressure is equal to the saturation pressure, boiling phenomenon occurs in which vapour bubbles begin to nucleate at the solid-liquid interface; outside of this condition however, evaporation largely occurs without any boiling effects.

Outside of saturation conditions, liquid to vapour phase change is heavily influenced by the behaviour of vapour developing at the interface and its diffusion into the environment. As the evaporation process occurs there is a natural tendency for vapour to saturate at the liquid-vapour interface thereby increasing the local vapour pressure and reducing the evaporation rate, particularly in the case of small sessile droplets due to its geometry. In the absence of any fluid motion in the gas phase, the driving mechanism for vapour transport is by diffusion. As described by Fick's law, the rate of diffusion depends on the concentration and diffusivity of the solute; thus for water vapour diffusing into air, the relative humidity is a limiting factor since the diffusivity remains relatively constant at atmospheric conditions. The diffusivity of water into air is 0.26 cm^2/s [5] and can be considered substantially slower than even the smallest forced air flows. While evaporation has been traditionally viewed as a *vapour-diffusion limited* process, forced removal of vapour would introduce advection rates higher than what is possible through diffusion alone, and can potentially raise the rate of evaporation.

In order for a molecule in the bulk liquid phase to overcome the attractive forces from surrounding molecules and leave the liquid-vapour interface, energy input is required [6]. This energy used to transition from liquid to vapour is known as the latent heat of vaporization. By extension of this principle, the evaporation rate of a liquid corresponds directly to the rate of heat removal from the surrounding environment. Energy for this process must come from either within the bulk liquid, the solid substrate, or surrounding gas phase. Thus, the magnitude of this energy transport has a significant influence on the rate at which evaporation occurs. As energy is consumed by the evaporation process, the localized temperature of each phase will potentially decrease. This decreasing temperature delta will subsequently reduce the rate of heat transfer by conduction. In the case of droplet evaporation, the reduction in heat conduction rate from the gas phase may be mitigated by a constant replenishment or motion of the gas. Meanwhile, temperature gradients in the liquid phase induced by this evaporative cooling effect will produce small density gradients, which could lead to buoyancy-driven convective flows. Surface tension is

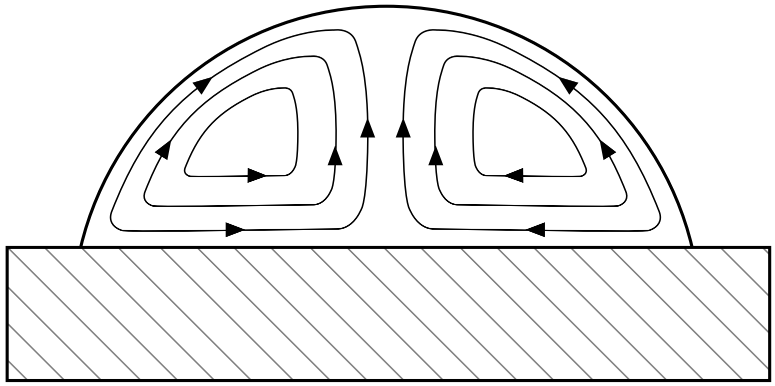

Figure 2: Potential internal flow patterns induced by buoyancy-driven or thermocapillary effects.

also a temperature dependent property, with an inverse proportionality, thus potential temperature gradients in the liquid will induce surface tension driven flows, also known as thermocapillary or Marangoni flows [6]. These internal convection effects can induce circulatory convection cells similar to those illustrated in Figure 2. At the same time, these effects must compete with the viscous and/or inertial forces present in the fluid. The interaction of these effects are highly dynamic and remain a point of interest for research in this field. The various internal flow regimes of the liquid phase will influence the energy transport by convection, and thus exert significant influence on the overall evaporation rate.

For engineers and designers considering applying droplet evaporation to practical systems, the mechanism to how droplets evaporate and its surroundings are also important. During the evaporation process of a liquid sessile droplet, the volume will decrease with time since liquid must leave the surface and into the atmosphere. Naturally, for a dry-out droplet, the resulting droplet shape changes and ultimately changes the internal flow patterns, altering the evaporation rate and energy transport mechanisms. In contrast during human perspiration, sweat is secreted out of pores in the skin, and may be continuously replenished by the body. For these types of continuously-fed droplets, the mass and energy transport mechanisms may be drastically different compared to dry-out droplets, owing to the steady droplet shape and potentially different internal flow patterns. Bioinspired evaporative cooling systems will need to be able to continuously supply liquid into the droplet to maintain heat removal rates and prevent dry-out. In addition, practical designs will necessitate the use of multiple droplets or large droplet arrays. The presence of adjacent droplets can influence not only the evaporation process due to additional vapour, but also alter the behaviour of any incoming air flows. Understanding these physical considerations are crucial towards increasing or optimizing droplet evaporation rates.

1.2 Literature Review

The following section presents a review of literature regarding sessile droplet evaporation. Given the wide-range of approaches undertaken by researchers around the world, the works discussed here are focused on experimental investigations into the evaporation of sessile droplets and its various influences. The first part presents some of the earliest works undertaken to establish the vapour-diffusion limited model of droplet evaporation, which is then followed by research on the effects of substrate thermal properties and heated substrates on the evaporation rate. Next, several works regarding the influence of the ambient environment and natural convection of vapour are presented, followed by a discussion of various studies which experimented with continuously-fed droplets. The subsequent section provides an overview of papers which have investigated the influence of moving gas, or forced convection, on the evaporation of dry-out droplets; a short discussion on other forms of droplet evaporation under forced convection is also provided. Finally, the gaps in current literature are identified and a summary of thesis objectives is provided.

1.2.1 Vapour-Diffusion Model of Sessile Droplet Evaporation

The evaporation of sessile droplets is a complex process; various approaches have been taken in the past to elucidate the underlying heat and mass transfer processes, and numerous attempts have been made to predict the rate of evaporation. Early studies have focused on establishing basic models to predict evaporation rates and droplet lifetimes, as well as determine which of the major geometric parameters are most important.

One of the first experimental studies into the evaporation of sessile droplets was conducted by Picknett and Bexon in 1977 [7], they had first established two main modes of evaporation; an initial constant contact radius mode in which the contact angle decreases with time while the contact line remains pinned, followed by a constant contact angle mode in which the contact line recedes while the droplet maintains a constant contact angle. From these observations, Picknett and Bexon proposed a theoretical model to predict the evaporation rate for a drying droplet limited by the diffusion of vapour into the surrounding gas. In 1989, Birdi et al. [8] conducted experiments which showed that the evaporation rate was linearly proportional to the droplet radius, and the constant radius mode dominated the lifetime of a drying droplet, therefore it was constant for the majority of the droplet lifetime. Birdi et al. subsequently developed a simple vapour-diffusion model to predict the evaporation rate,

$$I = 4\pi RD(c_0 - c_\infty) \tag{1.2}$$

where R is the droplet radius, D is the diffusion coefficient of water vapour into air, c_0 is the vapour concentration at the droplet interface, and c_∞ is the vapour concentration far away from the interface. Rowan et al. approached the vapour-diffusion model from a different perspective [9] by incorporating the spherical cap approximation. Their resulting model predicted a time dependence of droplet height and suggested that the evaporation rate is proportional to the height rather than radius, thus decreasing linearly with time until dry-out, directly contradicting the findings of Birdi et al. Within the same year, Bourges-Monnier and Shanahan published the results from a series of experiments [10] which suggested that the average evaporation rate decreases with an increasing initial contact angle, an observation also made by Picknett and Bexon. During the constant radius evaporation mode, very little difference in the evaporation rate was observed when the contact angle was greater or less than 90°. In 2002, Hu and Larson [11] published a study which used experimental results to develop a finite-element model (FEM) that solved for the vapour concentration distribution around the droplet and the evaporation flux over the liquid-vapour interface. From the results, an approximate expression for the evaporation rate was developed,

$$-\dot{m}(t) = \pi R D (1 - H) c_v (0.27\theta^2 + 1.30) \tag{1.3}$$

where R is the droplet radius, D is the diffusion coefficient of vapour into air, H is the relative humidity of the ambient air, c_v is the saturated vapour concentration and θ is the contact angle. This expression suggests a strong dependence on R, but a weak dependence on θ; for contact angles less than $40°$, the evaporation rate becomes nearly constant. Predictions made by this model also showed good agreement with the results published by Birdi et al., and the authors also concluded the evaporation rate remains almost constant over the lifetime of the drying droplet. Additional work by Hu and Larson was later done to model the internal flows within the droplet and determine the influence of Marangoni flows [12, 13]. It is clear from these studies that the diffusion of vapour plays an outsize role in determining the evaporation rate, while geometric parameters such as radius, contact angle and height play lesser roles; however, these vapour-diffusion limited evaporation models are only applicable to droplets evaporating completely.

While the vapour-diffusion model had thus far been relatively successful in predicting evaporation rates for certain cases, the influence of substrate thermal properties and energy transport from heated substrates remained unknown; yet understanding these influences are instrumental towards the design of heat removal technologies. In 2004, Crafton and Black [14] published results from experiments of water and

n-heptane droplets drying completely on heated copper and aluminum substrates which showed similar evaporation rates between the two materials, and remained constant during the droplet lifetime. They also observed that while larger contact radii increased evaporation rates, the resulting heat flux was lower. From these results, the authors suggested the use of numerous smaller droplets would have superior heat transfer compared to a single larger droplet. Another study published around this time by Mollaret et al. [15] showed that drying droplets on heated aluminum substrates experienced de-pinning at low temperatures which results in a deviation of evaporation rates from the vapour-diffusion model. Additionally, the evaporation rate on aluminum was clearly higher than on polytetrafluroethylene (PTFE). In 2007, Ristenpart et al. [16] showed that the direction of thermocapillary flows which induce continuous convection within the droplet were affected by the ratio of thermal conductivity between the liquid and the substrate. David et al. [17] conducted a series of experiments involving droplets evaporating completely on PTFE, macor, titanium and aluminum, which showed that evaporation rates on the metallic substrates were generally higher. However, evaporation rates between titanium and aluminum were nearly identical, even though the thermal conductivities of each material were an order of magnitude apart. Temperature measurements made by miniature thermocouples inside the droplet and immediately outside the interface suggested that the heat flux was limited by the substrate conductivity. Dunn et al. [18] expands on the work by David et al. by using the experimental results to include the variation in saturation concentration of vapour into the vapour-diffusion model of Hu and Larson, but results suggest that thermocapillary convection was not a significant contribution to evaporation rate. Energy transport from the substrate has been shown to affect the evaporation rate, increasing on high conductivity substrates, but these effects are only shown on drying droplets.

Other studies leveraged the use of infrared (IR) thermography to determine how substrate thermal effects might alter internal flows and affect the evaporation rate. Girard et al. published a study in 2010 [19] observing droplet evaporation on heated copper substrates using IR thermography. The evaporation rate was observed to increase over time; the authors suggested that the thinning of the droplet as it drys out reduced the thermal resistance, enabling higher energy transport. Near the contact line, the evaporative mass flux increased with time until the evaporation mode changed from constant radius to constant angle, at which point it remained constant. These results suggests that at the end of the droplet lifetime, thermal energy from the substrate does not generate any additional increase in evaporation rate. In 2011, Brutin et al. published an experimental investigation of droplet evaporation on a heated substrate using an IR technique [20], with a greater emphasis on the radiative properties of the fluid to determine thermal motion inside the droplet. Thermo-convective instabilities [21] developed around the periphery of the droplet as it evaporates under constant radius mode, but disappeared at low contact angles as the droplet almost dries completely, coinciding with a decrease in heat flux. Subsequently, Sobac and Brutin conducted an additional study [22] on water droplet evaporation on various heated substrate materials. Their experiments showed that the vapour-diffusion model under-predicts the evaporation rate in the hydrophilic case while over-predicting the hydrophobic case. A significant difference in evaporation rate was found between polyoxymethylene (POM) and the metallic substrates; but very little difference was found between tests on metallic substrates, corroborating the findings by David et al. Sobac and Brutin further suggested that rather than simply considering thermal conductivity, thermal effusivity, $\beta = \sqrt{k\rho c_p}$ which considers the density and heat capacity as well, may provide more insight into substrate influences. The use of IR in these studies demonstrated some of the internal convection effects for evaporating droplets, particularly as the droplet reduces in volume which causes different modes to occur.

A number of studies also attempted to determine the effects of the atmosphere on droplet evaporation, as well as the role that natural convection of vapour may have. In 2009, Kelly-Zion et al. used the Schlieren method to semi-quantitatively measure the extent of the vapour region above an evaporating droplet [23]. Substrates with pedestal geometries enabled greater vapour flows and increased the evaporation rate with height in contrast to well geometries which had an adverse effect. However, even for conditions where convection was observed to be the strongest, diffusion of vapour evidently remained the largest influence on evaporation rate. A second study [24] was later published which focused on flat substrates and droplets of various radii, from 1 to 22 mm. A combined diffusive and convective transport model was developed using the vapour-diffusion model and empirical correlations with Grashof number, that under-predicted the rates for methanol and acetone, suggesting that evaporation for these liquids may not be strictly limited by diffusion. In 2009, Sefiane et al. [25] published results which showed that the evaporation rate increases exponentially with decreasing gas pressure, while evaporative cooling of the liquid was more pronounced for low conductivity substrates at these pressures. They also showed that when evaporation occurs under an ambient gas with lower diffusion coefficients, the increase in evaporation rate on high conductivity substrates was reduced. Carle et al. published a study in 2013 [26] which involved experiments at terrestrial and micro-gravity levels. The evaporation rate predicted using the vapour-diffusion model was much more accurate for micro-gravity than in terrestrial gravity, which demonstrates that buoyancy-driven convective transport of the vapour significantly influences the evaporation rate. In a later study [27], Martian (0.38 g) and lunar (0.16 g) gravity conditions were also tested to improve the model, as well as the testing of various alkanes. In 2017, Misyura [28] showed that vapour-gas convection exerts significant influence on droplet evaporation in the absence of boiling; however, with droplets of aqueous salt solutions, this convective influence increases with the salt concentration of the liquid until a maximum is reached in the middle of the evaporation process, and decreases dramatically at the end of the droplet lifetime. These studies showed that buoyancy-driven convection of vapour increases the evaporation rate and may not be strictly vapour-diffusion limited, yet this effect varies under different gas conditions and droplet substances.

The aforementioned studies have been strictly concerned with droplets evaporating completely, i.e. drying out. However, the use of continuously-fed droplets is necessary for the design of heat removal applications and it cannot be assumed that evaporation characteristics under dry-out conditions would be the same here. C. A. Ward and colleagues developed an experimental method which used a syringe pump to supply water to a conical funnel [29, 30] for droplet formation, which was later adapted to continuously feed a droplet to a copper substrate [31]. Their experiments involved evaporation at vacuum pressures and was used to develop an alternate approach to evaporation rate prediction called Statistical Rate Theory. In 2014, Gleason and Putnam [32] used a laser to cut a ”moat-like” groove in an acrylic substrate to force pinning of the droplet contact line, enabling experimentation of contact angle dependence on evaporation. This experimental approach was later expanded [33] to include two grooves at different radii. Gleason et al. also used a syringe pump to continuously supply liquid to the droplet, and the pump rate was manually adjusted to maintain droplet height and angle. They found that larger contact angles under this ”steady-state” condition increased evaporation rates, but also increased thermal resistance. In 2017, Mahmud and MacDonald [34] experimentally measured the temperature within and immediately outside a continuously-fed droplet evaporating on a heated copper substrate. Two separate layers were used for the substrate with an inlet hole machined into the center and a groove around the top to establish contact line pinning, as shown in Figure 3. Their results suggested the existence of thermocapillary convection cells, which may exhibit different patterns depending on the substrate temperature, and may contribute up to 36% of the energy transport within the droplet. Zhong and Duan [35] published a study using an experimental technique similar to Mahmud and MacDonald, where a syringe pump is used to continuously supply liquid to a two-layer substrate. Their experiments use IR imaging to observe hydrothermal waves in continuously-fed droplets, which were shown to arise due to internal instabilities and increase in number as the substrate temperature increases; however, their influence on the evaporation rate remains unknown. Recently, Ye et al. [36] investigated the evaporation of a continuously-fed isopropanol droplet using a manual pump control technique similar to that of the previous authors discussed above. Their observations using IR imaging showed an increasing number of thermal wave patterns similarly to Zhong and Duan, and their evaporation rate measurements showed higher rates on copper than aluminum substrates; suggesting that substrate thermal properties may play a larger role in continuously-fed droplets. Various approaches have been taken by these studies to produce continuously fed droplets, yet all of these methods involve manual control of the liquid supply, and results suggest different internal convection behaviour during evaporation.

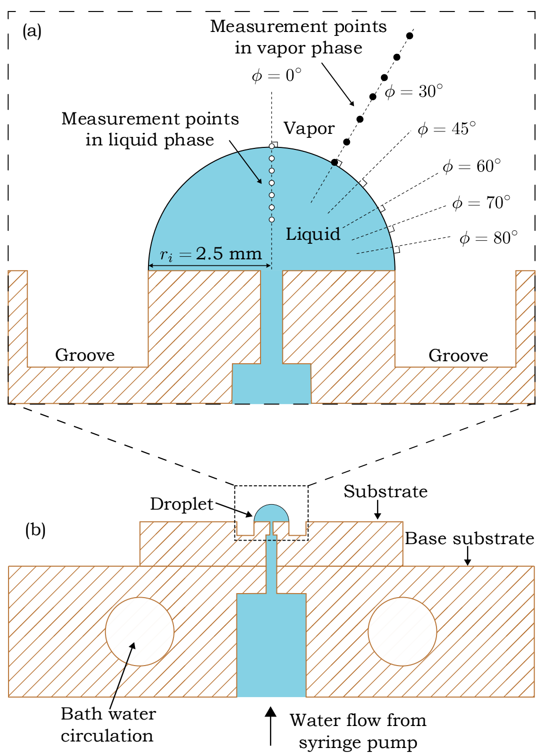

Figure 3: Experimental apparatus used for continuously-fed droplet, displaying temperature measurement locations in the liquid and vapour phases. Reproduced from [34].

1.2.2 Droplet Evaporation Under Forced Convection

Sessile Droplets Under Forced Convection

Investigations into the mechanisms behind droplet evaporation have largely focused on vapour-diffusion limited cases where vapour saturates around the droplet. However, applications involving thermal management will often occur under the influence of moving gas flow, either due to atmospheric conditions or induced by fans and blowers. A few authors have investigated their effects on the evaporation of drying sessile droplets.

In 2008, Navaz et al. [37] conducted experiments to determine the influence of turbulent effects on the complete evaporation of chemical agent HD (Mustard). Their approach used a friction velocity determined from wall shear stress, free-stream velocity and turbulence intensity measurements to develop an evaporation master curve for predicting evaporation times under a wide variety of conditions. Results from the experiments showed that air temperature has a significant influence on the evaporation time, but this effect may be suppressed by increasing free-stream velocity or turbulence intensity to promote convective transfer. Bin et al. [38] published a study in 2011 which monitored the evolution of droplet size and shape under various imposed air velocities. Their results showed that in all three evaporation stages, the evaporation rate was found to increase with air velocity, with the highest rate occurring during the constant angle mode before transitioning to constant radius and subsequently drying out. In 2016, Isachenko et al. [39] published results from experiments on water droplets evaporating on a stainless steel plate placed within a small scale

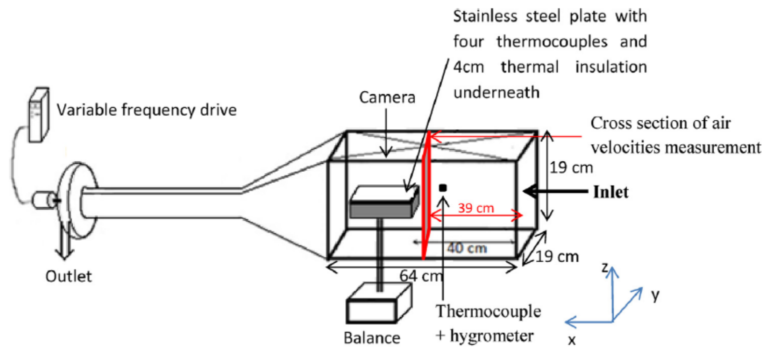

(a)

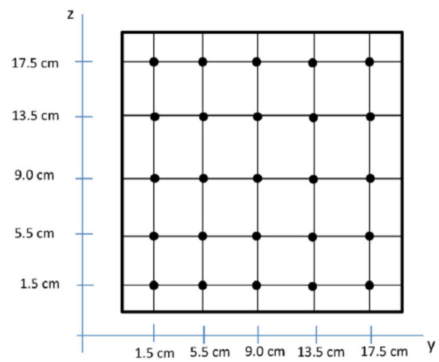

(b)

Figure 4: Schematic representation of wind tunnel, a) position of the cross section, b) positions of thermocouple measurements. Reproduced from [40].

wind tunnel, showing that substrate temperatures were more influential at higher velocities. Around this time, Lecoq et al. [40] published a study on the evaporation of droplet arrays under forced convection inside a wind tunnel, as shown in Figure 4. Experiments involved the complete drying of the steel plate, and unpinned droplets for larger wetted surfaces formed large films rather than remain droplets. Results also suggested that air velocity has a smaller effect on the evaporation rate compared to the temperature delta between the air and substrate, increasing with a larger wetted surface. Doursat et al. [41] expanded on the work by Lecoq et al. by conducting additional experiments with stainless steel and PVC substrates, and used the data to validate a numerical model which takes into account the coupled heat and mass transfer mechanisms. Experiments involving forced convection have shown reductions to evaporation times of drying droplets, although these effects to the evaporation rate are unclear for continuously-fed droplets.

A few authors had also directly compared evaporation times of drying droplets with and without forced convection directly over the droplet. In 2006, Shahidzadeh-Bonn et al. [42] published a study comparing the evaporation of water and hexane, showing an exponential dependence of evaporation time on the droplet radius for water. In particular, confining the droplet appeared to remove this exponent. Alternatively, hexane droplets did not exhibit this exponential dependence until a forced air flow is imposed directly over the droplet. In 2016, Carrier et al. [43] published a study on the evaporation rates of single droplets and droplet arrays. Their results found that in droplet array cases, droplets in the periphery evaporated faster, and developed a "super-drop" approximation to predict evaporation rates. They revisited the effects observed by Shahidzadeh-Bonn et al. to determine a critical radius where natural convection becomes the dominant transport mechanism; experiments with a fan blowing directly over the liquid appeared to cause this transition to occur earlier.

Other Droplets Under Forced Convection

The preceding section has reported a number of experimental studies on the effects of forced convection on sessile droplet evaporation. However, there exists a separate body of work concerned with suspended or fully immersed spherical drops under gas flow. In 1952, Ranz and Marshall [44] published the seminal work detailing experimental results on the evaporation of suspended spherical droplets in gas flows of various velocities and temperatures. The results of their study and Nusselt number correlations they produced have been widely sourced and used in many subsequent works. Studies concerned with spherical droplets in gas flows often focus on the evaporation and vaporization of fuel droplets [45–48] or droplets immersed in high temperature/pressure gas flows [49–53] intended for combustion applications. The absence of a solid-liquid interface in the case of immersed droplets leads to significant differences in heat transfer characteristics compared to the evaporation of sessile droplets. Therefore, the relevant energy transport mechanisms and droplet flow characteristics are not present in these cases, and thus a full review of literature in this field is beyond the scope of this thesis.

1.3 Gaps in Current Literature

The phenomenon of sessile droplet evaporation has been extensively studied in the past several decades to understand the underlying heat and mass transport characteristics. Through rigorous experimentation and analysis, the vapour-diffusion limited model of evaporation has remained the most widely used approach for predicting droplet evaporation rates. Various authors have looked at the different influences on evaporation rates, including geometric parameters such as droplet height, contact radius and contact angle, with Hu and Larson concluding the strong influence of radius and weak influence of contact angle in their model [11]. Other researchers have investigated the influence of substrate thermal properties and energy transport from heated substrates, finding that higher conductivity substrates generally enhance evaporation rates [15, 17, 22]. The effects of natural convection and influence from the ambient environment has also been investigated, as well as evaporation characteristics of continuously-fed droplets, but specifically in the absence of any external convection. There have also been studies which considered the influence of induced gas flow, or forced convection, on the droplet evaporation rate, but all of these cases involve droplets drying out completely.

From the review of current literature to date, it appears there has yet to be any investigation into the influence of forced convection on the evaporation of continuously-fed sessile droplets. Furthermore, current models to predict evaporation rates mainly rely on the assumption of being vapour-diffusion limited, without much consideration for the consequences of removing this limit. An experimental investigation into this case can provide valuable data for the design and optimization of thermal management technologies that could leverage this artificial perspiration technique.

1.4 Thesis Objectives

The objective of this work is to experimentally investigate the influence of a moving gas flow, or forced convection, on the evaporation of a continuously fed sessile droplet and determine whether other limits exist beyond the widely assumed vapour-diffusion limit. The main objectives of this work are:

- Develop and construct an experimental method and apparatus to create accurate and consistent air flow over a continuously fed sessile droplet and facilitate measurements of evaporation rate

- Determine the influence of air velocity on the evaporation rate on a single droplet
- Determine whether the evaporation rate is affected by surrounding droplet features

Chapter 2

Experimental Apparatus and Methods

This chapter discusses the design and construction of the experimental apparatus used for this thesis. There were three main challenges addressed in the development of this experiment:

(i) Formation of a pinned droplet with a continuous liquid supply

(ii) Provide stable and accurate laminar flows to determine air velocity influence

(iii) Control of droplet shape under dynamic conditions while facilitating the measurement of evaporation rates

2.1 Apparatus Overview

An illustrated schematic of the experimental setup can be seen in Figure 5. The setup consists of a small scale low-speed wind tunnel built for this experiment, de-

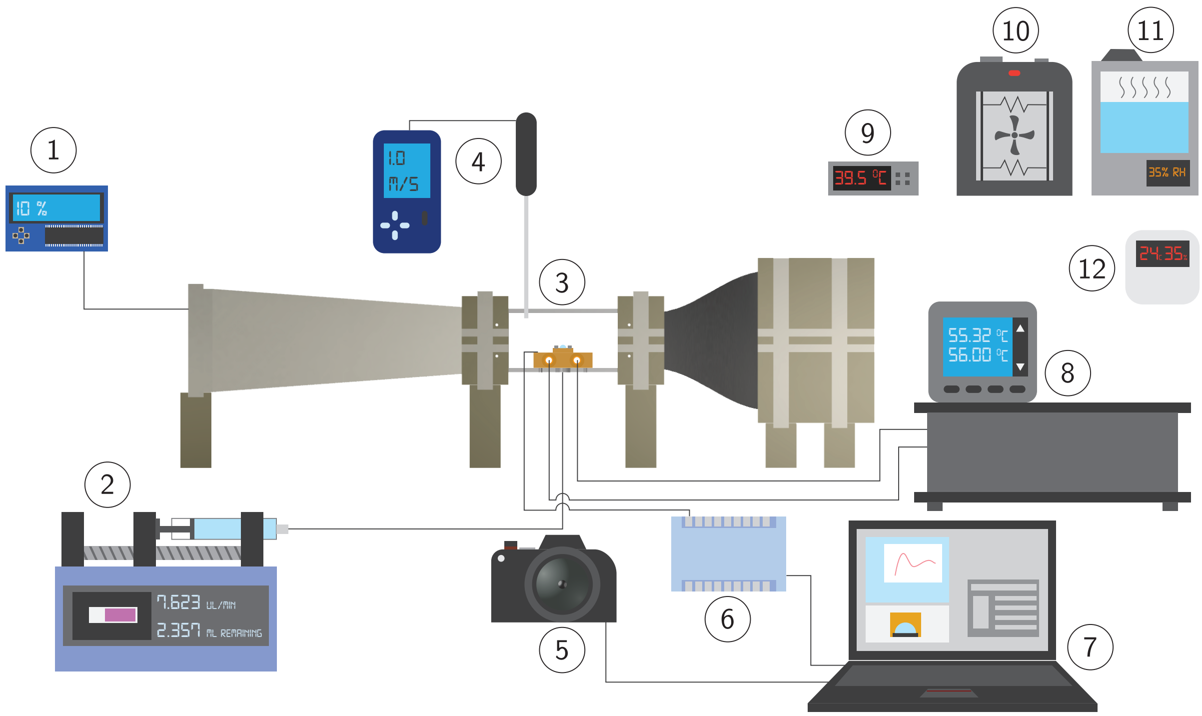

Figure 5: Illustrated schematic of the experimental setup. 1) Arduino fan controller, 2) Syringe pump, 3)Wind tunnel with droplet substrate, 4) Hot-wire anemometer, 5) DSLR Camera, 6) DAQ module, 7) Laptop Computer, 8) Hot water circulation bath, 9) Temperature controller, 10) Space heater, 11) Humidifier, 12) Thermometer/Hygrometer

tails of the design are outlined in section 2.3. Inside the wind tunnel test section is the copper substrate which forms the droplet, discussed in section 2.2. A syringe pump (Harvard Apparatus Pump 11 Elite) is connected to the droplet substrate from below and supplies distilled water via a glass syringe (Hamilton 1005-TLL). A hot water circulation bath (VWR AD07H200) is connected to the substrate to circulate hot water for maintaining substrate temperatures. Air velocity in the wind tunnel test section is measured using a hot wire anemometer (PCE-423). A DSLR camera (Nikon D5200, lens: Nikon AF-S Micro Nikkor 60 mm f/2.8G) is used to capture images and connected to a laptop computer for image processing. A T-type thermocouple is connected to a data acquisition device (Omega OM-USB-TC) to record temperature measurements of the substrate. A temperature controller (ITC-1000F) is connected to a ceramic space heater (AmazonBasics DQ078) to maintain ambient air temperatures, and a humidifier (Taotronics TT-AH001) was used to maintain relative humidity levels. A separate thermometer/hygrometer (Traceable 4088) was used to verify ambient conditions. The experimental equipment is contained within a 1.17 m $\times$ 0.81 m $\times$ 1.79 m enclosure constructed using construction lumber and polyethylene sheeting to maintain various air temperatures and relative humidity levels; two additional small USB fans were placed within the enclosure to ensure even air circulation. A zippered door was cut into the sheeting to enable access into the enclosure during experiments. The enclosure and equipment contained inside was mounted onto an anti-vibration optical table (Thorlabs Nexus) with the exception of the hot water circulation bath; this was done to isolate the experiment from vibrations caused by the circulation bath pump and external environment. A photograph of the experimental setup is shown in Figure 6 to provide an accurate representation of equipment placement.

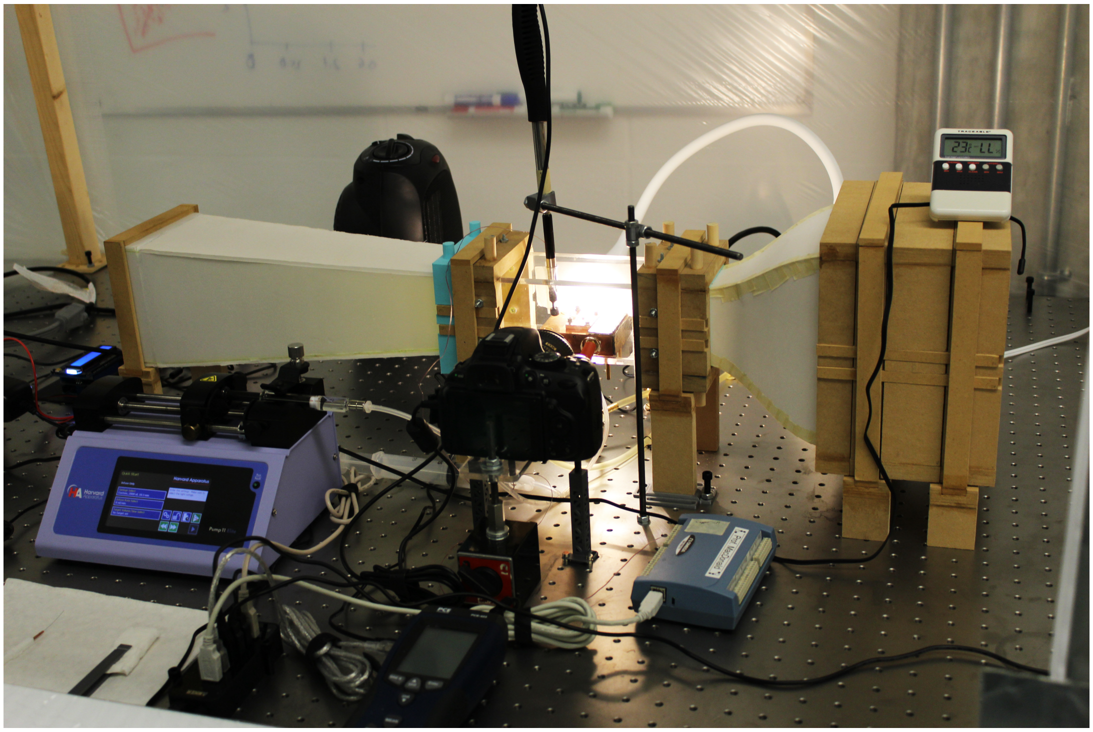

Figure 6: Photograph of the experimental setup.

2.2 Droplet Formation and Substrate Design

The substrate design must accomplish three main goals; provide an isothermal surface for evaporation, enable droplet formation with a continuous liquid supply, and pin the contact line of the droplet to a fixed radius. Providing an isothermal surface for evaporation eliminates any temperature gradient in the substrate that may alter conduction rates or convective behaviour. The substrate is constructed from pure copper and consists of an upper "feeder" block and lower "heater" block; the substrate assembly is shown in Figure 7. The heater block measures 53.5 mm × 75 mm × 19 mm and has two 8.5 mm diameter channels machined through the sides. At the ends of each channel is a 1/4″ NPT barbed fitting connected to the hot water circulation

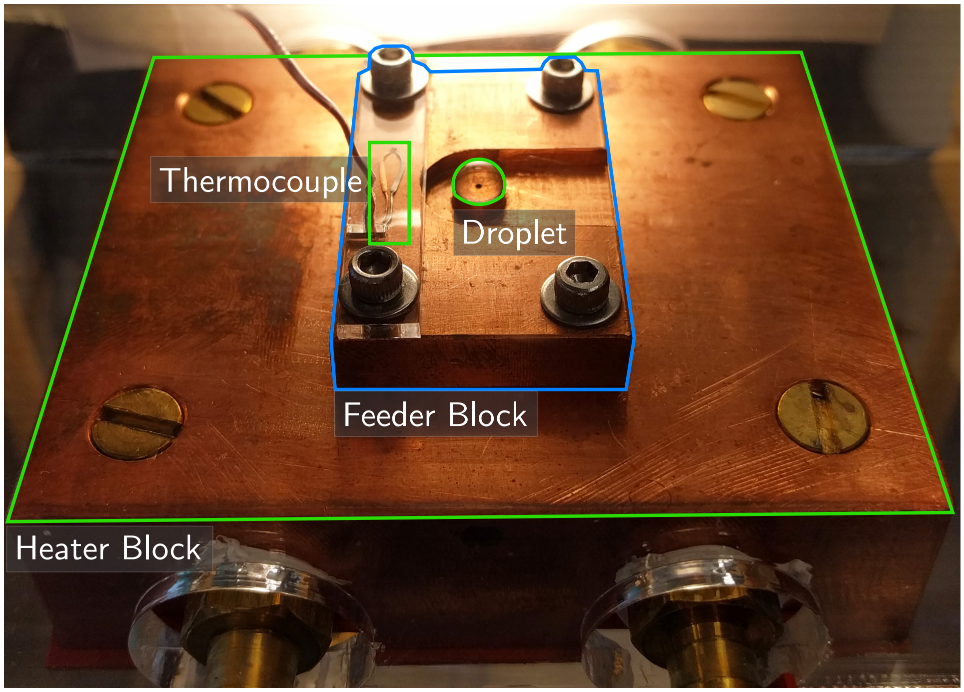

Figure 7: The substrate assembly for droplet formation, shown with the $R = 2.5$ mm droplet feeder substrate.

bath in a cross-flow arrangement. The use of copper ensures that as hot water is fed through these heating channels, the substrate maintains a constant temperature. Another hole was machined through the center for supplying fluid to the upper feeder block. The two-piece design of the substrate enables usage of separate feeder blocks for different droplet radii, as shown in Figure 8. The feeder block measures 33 mm $\times$ 20 mm and has a center hole with a diameter of 0.35 mm for fluid supply. Droplet pinning is achieved by machining a pedestal at the center around the fluid inlet; the edge of the pedestal constrains the droplet radius and fixes the contact line. In addition to droplet pinning, the feeder substrate surface was machined away at a depth of 3 mm, in the frontal area upstream of the pedestal for the 2.5 mm droplet, and the entire surface for the 1.25 mm droplet substrate. This was done to eliminate any potential boundary layer effects; the boundary layer height was approximated as

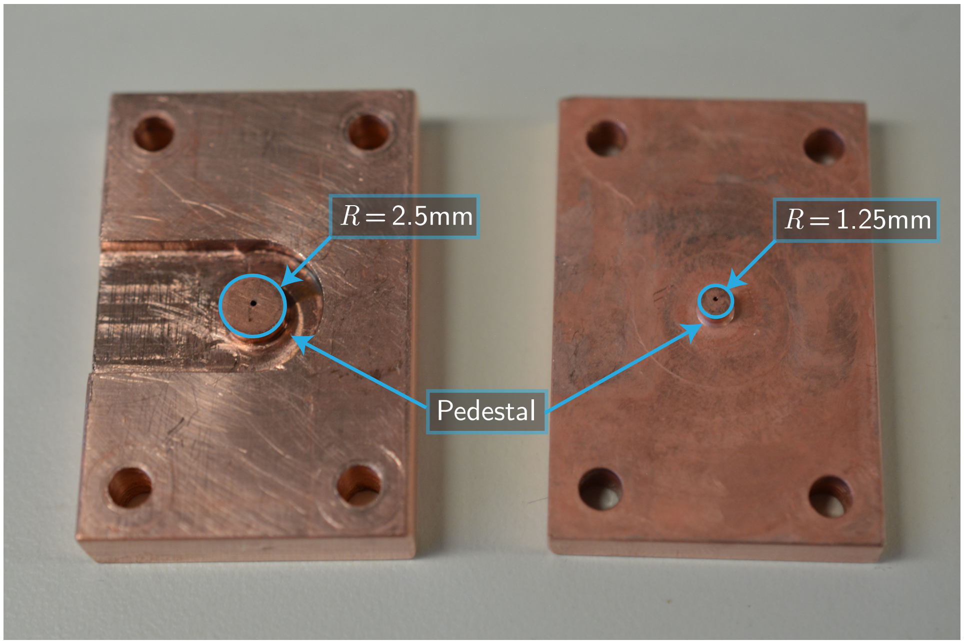

Figure 8: Two "feeder" block portions of the substrate. Block on left was used for $R = 2.5$ mm droplets, block on right was used for $R = 1.25$ mm droplets.

that of a flat plate [54] according to

$$h = 4.9\sqrt{\frac{\nu x}{U}} \tag{2.1}$$

where ν is the kinematic viscosity of air, x is the distance from the leading edge to the pedestal, ≈ 12 mm, and U was the air flow velocity, taken as 0.5 m/s, which is close to the lowest possible velocity and accounts for the largest boundary layer height. A T-type thermocouple is clamped to the substrate directly behind the droplet pillar using an acrylic clip to measure substrate temperatures.

2.3 Wind Tunnel Design and Construction

A custom bench-top wind tunnel was constructed to produce the experiment conditions required. The tunnel is an open-loop design in a suction configuration; air is not explicitly recirculated and the fan driving air flow is placed downstream of the test section. The wind tunnel provides consistent laminar flow conditions for experimental testing; turbulent effects caused by unconditioned flows would introduce significant errors to the analysis of the relationship between air velocity and evaporation rates. An open-loop configuration is the simplest to construct and by placing the wind tunnel within a sealed enclosure, air temperature and humidity levels may be controlled using off-the-shelf components rather than custom solutions necessitated by space constraints in a closed-loop configuration.

The wind tunnel assembly consists of: a flow conditioner, polynomial contraction, test section, and diffuser; a schematic is shown in Figure 9. Structural framing for the flow conditioner and between each section was designed with CAD modeling software

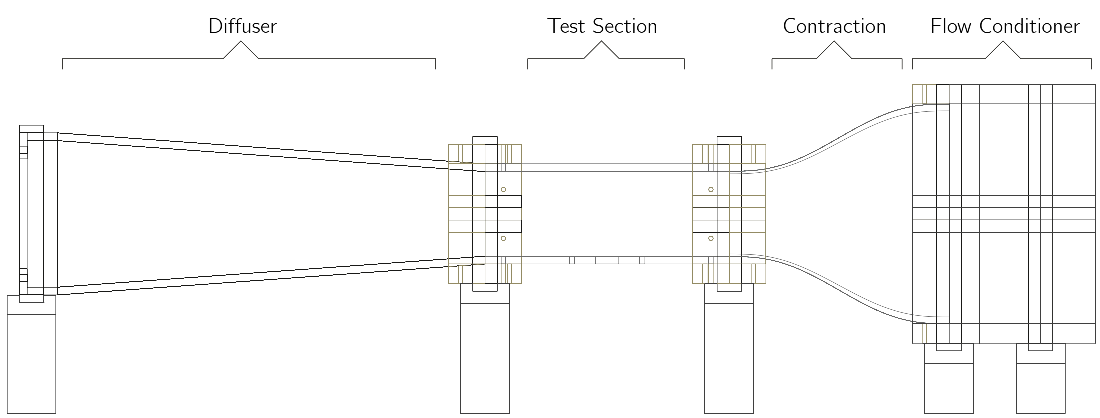

Figure 9: A wire-frame schematic of the wind tunnel denoting each section.

(Unigraphics NX9) and CNC-machined from medium-density fiberboard (MDF) on a bench-top CNC mill (Shapeoko 3).

The flow conditioner consists of three stages, a honeycomb at the inlet followed by two fine mesh screens; the purpose of these components are to minimize swirl and lateral velocity variations, and break up potential turbulent eddies. The honeycomb was constructed from 5 mm diameter plastic drinking straws cut into 40 mm sections to achieve an optimal cell length-to-diameter ratio of 8 [55]. The mesh screens were produced from card stock by cutting a mesh pattern using a laser cutter (Trotec Speedy 100). The first mesh screen consists of 2 mm diameter holes spaced 2.5 mm apart, the second screen consists of 1 mm diameter holes spaced 1.25 mm apart. The first screen is located 50 mm downstream of the honeycomb (10 cell diameters), and the screens are 25 mm apart (25 mesh cell diameters). The settling chambers formed between screens allow for turbulent effects to dissipate prior to encountering the next screen [55, 56]. The honeycomb and screens are shown in Figure 10.

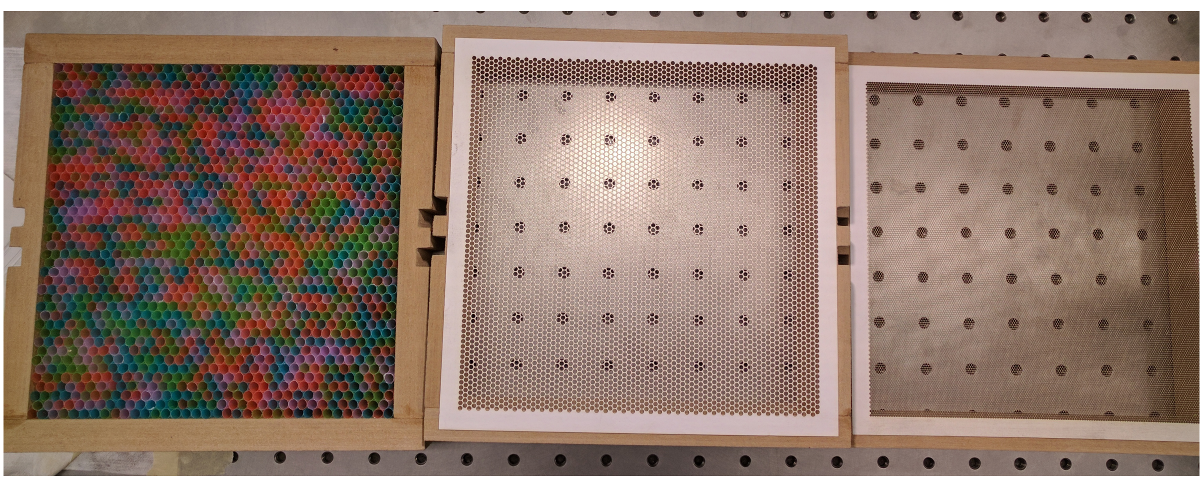

Figure 10: Flow conditioner components. Left: honeycomb, middle: 2 mm mesh, right: 1 mm mesh

The contraction is located downstream of the flow conditioner and increases the mean flow velocity as well as reducing the mean and fluctuating velocity variations [55]. The contraction shape is 3-dimensional and the contour is a 5$^{\text{th}}$ order polynomial shape developed in [57],

$$y(x) = h_i - (h_i - h_e)[6(x')^5 - 15(x')^4 + 10(x')^3] \tag{2.2}$$

where h_i is the inlet height (180 mm), h_e is the exit height (70 mm) and x' is the distance, x, normalized over the total contraction length, L (140 mm). The length-to-inlet-height ratio of the contraction is 0.77 to avoid flow separation and the contraction area ratio is 6.6. While Bell and Mehta found optimal results with a contraction ratio of 8, the ratio used here falls within the recommended range of 6-10 for wind tunnels featuring test section areas less than 0.5 m^2 and air velocities less than 40 m/s [57]; additionally, the maximum air velocity in their tests was 15 m/s which is significantly higher than the maximum 4 m/s used in the following experiments. The smaller contraction area ratio used here is mainly due to size constraints.

Downstream of the contraction is the test section which measures 200 mm × 70 mm × 70 mm and was constructed from laser cut acrylic; holes for were cut out to allow for the substrate fluid fittings. The diffuser is located downstream of the test section for pressure recovery, and in this design, housing of the fan at the diffuser exit. The diffuser length is 350 mm and expands from an entrance height of 70 mm to 120 mm to accommodate the fans used; this corresponds to a diffuser angle of 4° which is less than 5°, at which point flow separation and unsteadiness would occur [55]. Two different computer case fans (Insignia NS-PCF1250, Noctua NF-F12) were used to provide air flow. An Arduino Uno microcontroller was set up to provide pulse-width modulation (PWM) control to the fans for fine-tuning of air velocities. An analysis of data produced during an experiment at the highest air velocity, 4 m/s, shows a turbulence intensity, $\frac{U'}{U_{avg}} = 0.058\%$, where U' is the standard deviation of air velocity fluctuations, and U_{avg} is the average air velocity; this demonstrates the effectiveness of the wind tunnel design for producing laminar flows.

2.4 Computer Vision Method for Droplet Control

A control algorithm was developed to measure the droplet evaporation rate and facilitate data recording and equipment control. Unlike the gravimetric techniques used for droplets drying completely, which measure the reduction in mass over time, the droplet mass remains constant due to the continuous supply of fluid for continuously-fed droplets. Instead, the supply or flow rate of the pump may be equated to the evaporation rate of the droplet due to mass conservation, $\dot{m}_{pump} = \dot{m}_{evaporation}$, as long as the droplet shape remains constant. In experiments on continuously-fed droplets conducted by previous authors as discussed in the literature review [33–36], manual, trial-and-error methods were used to determine the syringe pump supply rate. This approach, while likely time-consuming, has demonstrated reasonable accuracy in determining evaporation rates in a quiescent environment. However, the dynamic conditions present under forced convection pose a significant challenge in estimating pump flow rates; at higher velocities, the droplet interface exhibits small oscillations caused by the air flow, making manual approaches nearly impossible. Additionally, the droplet substrate and wind tunnel prevents the use of commercially available droplet analysis solutions designed for simple drying cases. Therefore, a custom program was developed to obtain and process the droplet image, measure the droplet height, and automate pump control to determine evaporation rates.

Additional steps were taken to set up the camera and test section to enable visualization of the droplet and measurement of the evaporation rate. Inferring the evaporation rate from the pump flow rate requires the droplet volume to remain constant; since the droplet radius is constrained by the pedestal geometry, if the droplet height is held steady and remains constant with time, the droplet volume must also be constant. Water is naturally translucent and renders the interface, and therefore droplet height, difficult to detect. An LED lamp was placed level with the substrate base and directed at the droplet; a sheet of paper was attached to the test section wall to diffuse the light and avoid any optical interference to the camera. This light placement causes a shadow to outline the liquid-vapour interface. An adjustable-height tripod mount was constructed to accurately position and level the camera so that the centre of view is directed at the interface and also to reduce any parallax distortion.

A program was written in Python v2.7 to facilitate the image processing, pump control, and data collection. Python is a general-purpose, open-source programming language with a large collection of readily available libraries submitted by users worldwide; its interoperability with different software and hardware interfaces makes it particularly suitable for this application. For equipment control, direct camera interfacing, i.e. camera settings and image capture, was accomplished using a separate open-source software, digiCamControl. The Harvard Apparatus Pump 11 Elite syringe pump used for liquid supply was controlled using supported terminal commands over USB serial communication, a Python library published to Github was adapted to support the specific syringe pump model used here [58]. The open-source computer vision library, OpenCV, was used to conduct the necessary image processing. Data analysis libraries Numpy and Pandas was used for data collection and processing. The droplet control program does the following:

1. Communicate with the camera via digiCamControl and capture an image of the droplet
2. Process the image using OpenCV to obtain the droplet height
3. Communicate with the pump and adjust the flow rate using PID control
4. Record and save the data, and repeat

A computer vision technique was implemented using OpenCV to analyze images captured by the camera and determine the droplet height, the intermediate steps to this process is shown in Figure 11. First an image is captured and cropped to isolate the droplet region. The OpenCV function `cv2.cvtColor()` converts the image into greyscale, or black and white. This step is necessary in order to apply thresholding to the image, implemented using `cv2.threshold()` with the `THRESH_BINARY` parameter. Thresholding is a standard image processing technique which compares the pixel value to a predefined threshold value and assigned either a maximum (white) or minimum (black) value. This step outlines the droplet edge and removes any grey regions that

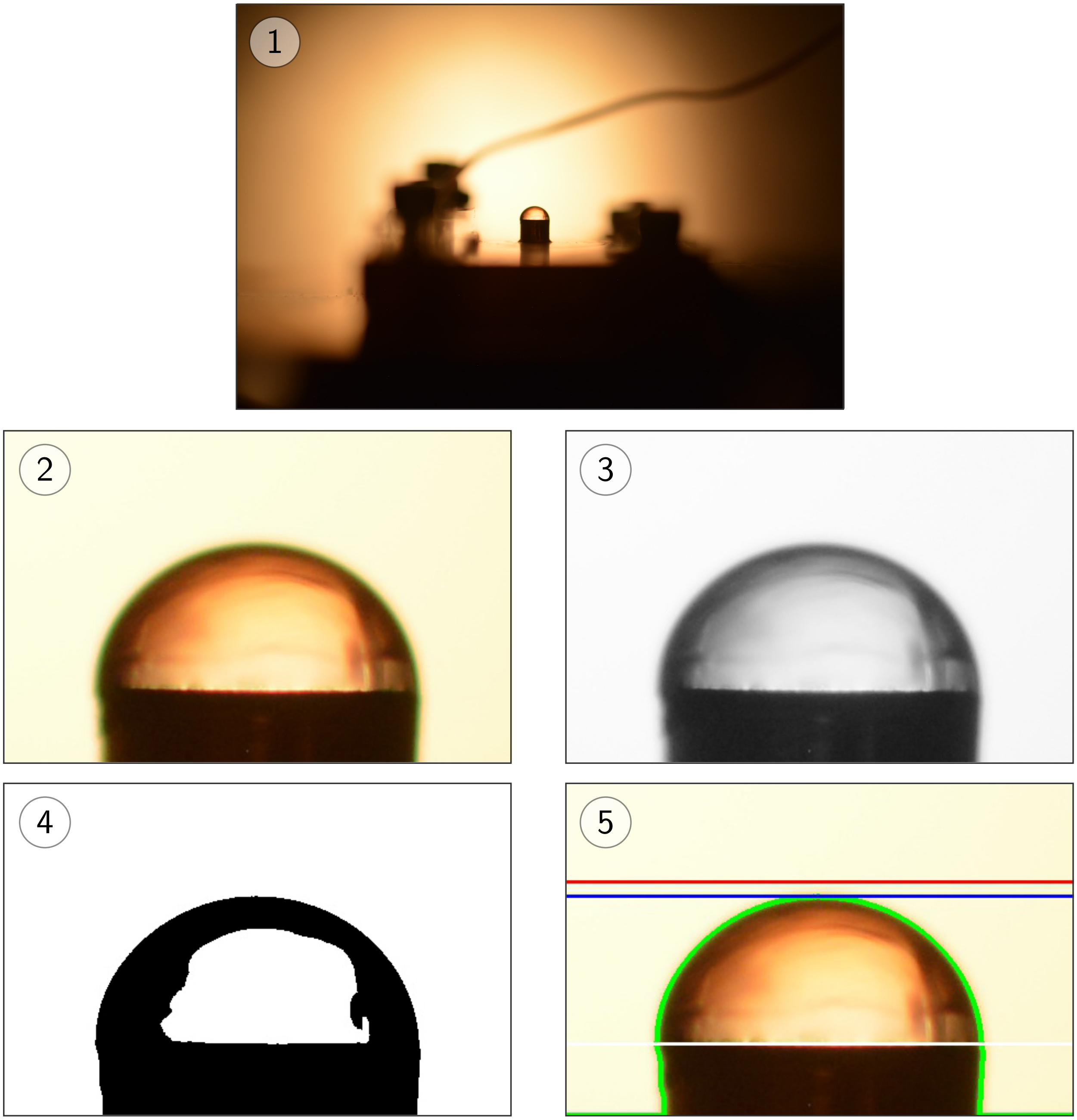

Figure 11: Image processing procedure to determine the droplet height. $R = 1.25$ mm droplet shown. 1) Image captured from the camera, 2) Cropped image, 3) Image converted to greyscale, 4) Thresholding applied to image, 5) Cropped image with traced contour shown in green, target droplet height line in red, substrate line in white and droplet height line in blue.

would otherwise obscure the contour-mapping. The function `cv2.findContours()` traces the contours in the image using this algorithm [59] and stores them as vectors of points in pixel coordinates. In order to convert pixel coordinates to millimetres, an image of a 1.5 mm tall acrylic calibration block is used to obtain a millimetre/pixel conversion ratio. The apex of the droplet is then determined from the vector array produced from `cv2.findContours()`. The location of the substrate is visually calibrated and used to determine the droplet boundaries alongside the user-inputted target height. A real-time output of the image and droplet location is implemented using the `matplotlib` library to monitor progress during experimentation.

A simple Proportional-Integral-Derivative (PID) controller was adapted from [60] to facilitate syringe pump control. Measured droplet height values were used as the process variable and pump supply/infusion rate was adjusted as positive control; pump infusion was reduced during overshoot and evaporation of the droplet was used as negative control. PID constants were determined experimentally through manual loop-tuning. The average refresh rate was ≈ 0.25 Hz, i.e. one image was captured every ≈ 3.5 s. This was due to the use of a DSLR camera for image capture, which has a slower mechanical shutter compared to CCD cameras, but allows the use of a high resolution macro lens at low cost.

2.5 Uncertainty and Sources of Error

The main sources of error and uncertainty are a result of the measurement tools used. Table 1 summarizes the accuracy for each measurement tool.

Table 1: Measurement tool accuracy

Measurement tool	**Parameter**	**Error**
Hot wire anemometer	air velocity (m/s)	±5% ±1 digit of measured value
T-type thermocouple	substrate temperature (°C)	±0.5 °C
Thermometer/Hygrometer	air temperature (°C), relative humidity (%RH)	±1 °C, ±5%RH
Temperature controller	air temperature (°C)	±1 °C

Determining the measurement error of the droplet control program is more complicated. The calibration block used to determine the millimetre/pixel conversion ratio was measured with ±0.02 mm accuracy. Camera settings were recalibrated regularly, and camera position would vary slightly; the average ratio used for height conversion was 0.0085 mm/pixel. The minimum process error of the PID control is 1 pixel, i.e. a single pixel difference between measured droplet height and target droplet height causes a change in pump infusion rate. The accuracy of the syringe pump was ±5%, with a minimum infusion rate of 1.26 pL/min, which is significantly less than the measured droplet evaporation rates. Aside from the uncertainties stated above, other sources of error are estimated to be less than the variance in the recorded data and deemed negligible. Each source of error outlined above contributes to the variations observed in the measured evaporation rates; therefore the error bars reported in the results and discussion are determined from the standard deviation of the data.

2.6 Experimental Method

Each experimental dataset is recorded using the process described in this section. A sample of distilled water is initially boiled on a hot plate for 10 minutes to reduce the amount of dissolved oxygen. The primary supply syringe and a secondary plastic syringe are both filled with the boiled distilled water and capped until connection to the fluid supply lines. A 5 % (v/v) acetic acid solution is heated on a hot plate and the copper substrate is left in the solution for 10 minutes to remove surface corrosion. The copper substrate is then washed with distilled water and a 96 % (v/v) isopropyl alcohol solution. Substrate cleaning was done between changing experimental parameters (i.e. air velocity). After cleaning, the substrate is assembled into the wind tunnel, and the syringes are connected; the secondary plastic syringe is used to pre-charge the fluid supply lines. The hot water circulation bath is set to the desired temperature and the substrate temperature is verified using thermocouple measurements. Next, the fan controller is set to the desired air velocity. The droplet control program is finally launched and the substrate location and droplet detection region is saved to the program settings. After the program has started, a minimum of 30 minutes was required to allow the PID control to settle at the correct evaporation rate, although for some of the experimental conditions, wait times were up to 2 hours. Data is recorded over a minute 15 period after the control loop had settled, and each experiment is repeated a minimum of 3 times. The data produced from the repeated experiments are then averaged to determine the evaporation rate.

Chapter 3

Results and Discussion

This chapter discusses the results of the experiment conducted according to the methods outlined previously. Initial experiments with the $R = 2.5$ mm droplet at various substrate temperatures and air velocities are discussed. Next, results from experiments with the $R = 1.25$ mm droplet are shown, highlighting a potential thermally limited case in the absence of a vapour-diffusion limit. This limiting condition is tested by experiments involving different ambient air temperatures at the same substrate temperature. Finally, results from tests investigating the influence of adjacent droplets on air flow behaviour is discussed.

3.1 Experiments on $R = 2.5$ mm Droplet

In this set of experiments, evaporation rates were measured for the larger radius droplet, $R = 2.5$ mm. Experiments were conducted under ambient laboratory conditions; the air temperature, T_a, was 24°C and relative humidity was maintained approximately 35%. Two sets of experiments were conducted with the larger droplet; the first set involves a range of substrate temperatures under a fixed air velocity, and the second involves a range of air velocities under a fixed substrate temperature. In both cases the droplet height is maintained at 2.5 mm; this corresponds to a Bond number of 0.87. In this Bond number range, the droplet maintains a rough hemispherical shape, but the influence of gravity causes the droplet to sag slightly into an oblate spheroid.

3.1.1 Constant Velocity and Droplet Height

For this experiment, the evaporation rate was measured for the $R = 2.5$ mm droplet on substrate temperatures ranging from 39°C to 74°C under an air velocity of 1 m/s; the results are shown in Figure 12. This preliminary set of experiments were conducted at the same substrate temperatures investigated by Mahmud and MacDonald in [34] to facilitate validation and comparison. However, it should be noted that the ambient air temperature reported by Mahmud and MacDonald was 30°C versus 24°C used in the current experiment. The results show that compared to a quiescent condition, removal of the vapour-diffusion limit and increase in air velocity results in significant increases to total evaporation rates. The relative increase is more significant at lower substrate temperatures; at substrate temperature $T_s = 39$°C, the evaporation rate under forced convection was larger by a factor of 2.6 while at substrate temperature $T_s = 74$°C, the increase in evaporation rate had diminished to a factor of 1.5. The general trend in both cases show an exponential increase in evaporation rate as substrate temperatures

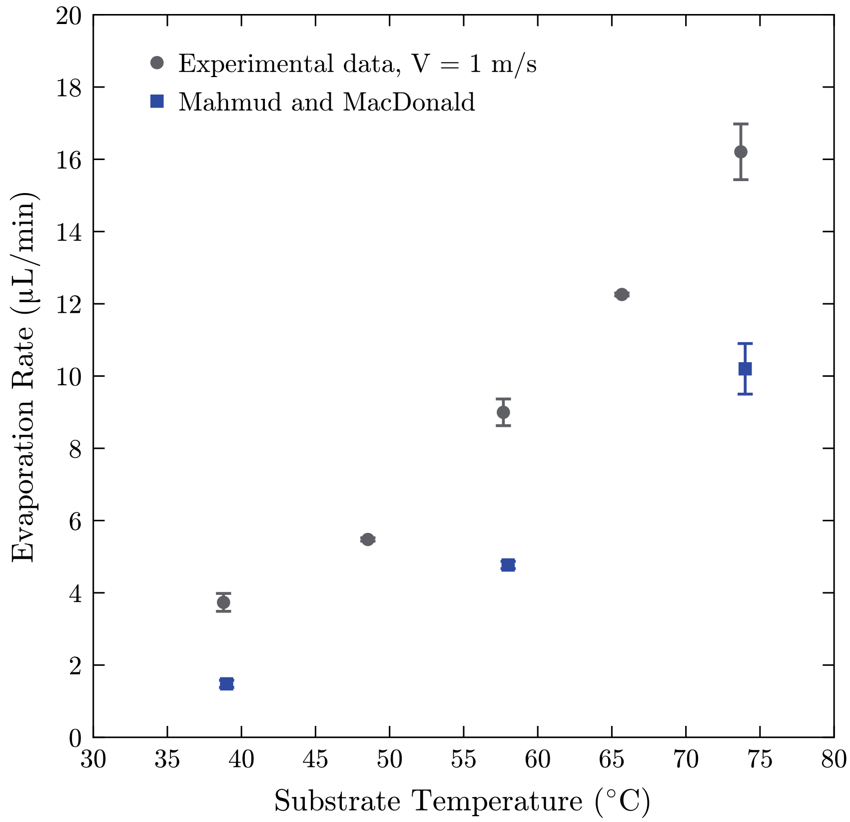

Figure 12: Evaporation rate measurements for the $R = 2.5$ mm droplet on various substrate temperatures from 39 °C to 74 °C. Air velocity is 1 m/s, and droplet height is 2.5 mm. Results are compared with evaporation rates measured under quiescent conditions from Mahmud and MacDonald [34]

increases. In general this comparison shows that forced convection can enhance the evaporation rate, and thus additional investigation is conducted on the effects of various air velocities.

3.1.2 Constant Temperature and Droplet Height

In the following set of experiments with the $R = 2.5$ mm droplet, the evaporation rate was measured at various velocities ranging from 0.7 m/s to 2 m/s. The substrate temperature was maintained at 55°C, which was the median value from the previous set of experiments, and generally correlates with operating temperatures of microchips and electronic components. As shown in Figure 13, the evaporation rate increases linearly with an increase in air velocity; the data is fitted to a linear regression, $Q_{evap} = 6.192 + 2.064U$ ($R^2 = 0.947$). The large error at the air velocity of 2 m/s is due to oscillations of the droplet interface. At this velocity, the momentum from the air flow is significant enough to cause the droplet to sway periodically, reducing

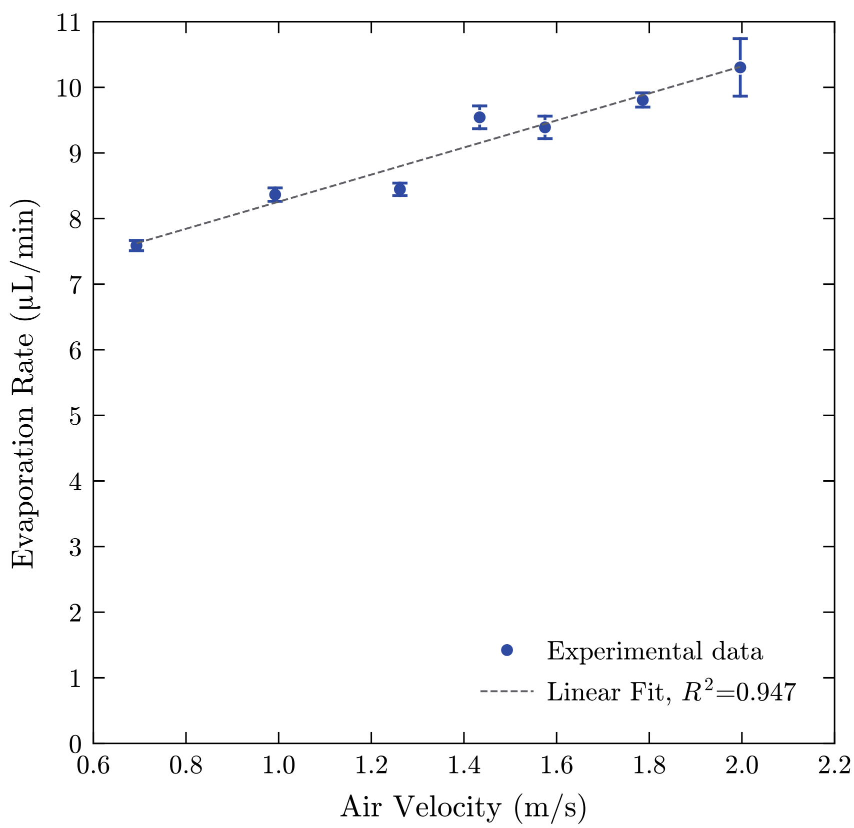

Figure 13: Evaporation rate measurements for the $R = 2.5$ mm droplet at various air velocities from 0.7 m/s to 2 m/s. Substrate temperature is 55 °C, and droplet height is 2.5 mm.

the accuracy of the droplet control program and evaporation rate measurement. The balance of fluid momentum from the incoming air flow and the surface tension effect constraining the droplet shape can be characterized by the Weber number,

$$We = \frac{\rho V^2 L}{\sigma} \tag{3.1}$$

where ρ is the liquid density, V is the air velocity, L is the characteristic length, taken as the droplet radius, and σ is the air-water surface tension; the Weber number for the $R = 2.5$ mm droplet and air velocity of 2 m/s is 142.

From these results, it appears that higher evaporation rates may be achieved by imposing larger air velocities. However, the potential limits to this mechanism and whether the evaporation rate would continue to increase at higher air velocities are unclear due to the physical limits of unsteady droplet motion. Therefore, further experimentation is conducted for a smaller droplet radius.

3.2 Experiments on $R = 1.25$ mm Droplet

In the following set of experiments, evaporation rates were measured for the $R = 1.25$ mm droplet. The initial experiments were conducted at the same ambient conditions as the previous cases. Additionally, experiments were conducted at an elevated air temperature to determine the influence of thermal effects. A final set of experiments were also conducted to investigate the influence of adjacent droplets and boundary layer effects. For the following experiments, the droplet height was maintained at

1.25 mm, which corresponds to a Bond number of 0.22, and thus the droplet retains a hemispherical shape unaffected by gravity.

3.2.1 Constant Temperature and Droplet Height

In this set of experiments, the evaporation rate for the $R = 1.25$ mm droplet is measured at various air velocities from 0 m/s to 4 m/s. The substrate temperature is maintained at 55°C, similarly to the previous experiment. The results are plotted in Figure 14. Comparing the evaporation rate at 0 m/s, which was measured with the fan off, and the rate measured at 1 m/s shows a smaller increase, a factor of 1.3 compared to 1.9 for the larger droplet; it should be noted that the substrate temperature is 3°C less in this case. This result may suggest that removal of the vapour-diffusion limit has a more significant effect for larger droplets. In the air velocity range of 0 m/s to 1.5 m/s, a linear increase in evaporation rate is observed, similar to the $R = 2.5$ mm droplet. However, measurements at 2 m/s show a deviation from this linear trend and a slight decrease. At higher air velocities, the evaporation rate shows small increases that remain deviated from the linear trend at lower air velocities. The measurement error at 3.25 m/s and 4 m/s are significant due to oscillation of the droplet interface caused by the air flow; the Weber numbers at these velocities are 187 and 284 respectively, which is comparable to the Weber number of 142 for the larger droplet at 2 m/s, suggesting that oscillatory motion becomes influential for Weber numbers $\gtrapprox 100$.

The evaporation rates of both droplet cases are plotted in Figure 15. From this comparison, it is clear that the increase in evaporation rate due to air velocity is more significant for larger droplet radii. At high air velocities, the evaporation rate for the $R = 1.25$ mm droplet reaches a plateau. This effect may be explained by considering the energy balance at the droplet interface,

$$q_{evap} = q_{cond} + q_{conv,i} - q_{conv,e} \tag{3.2}$$

where q_{evap} is the energy removed by the evaporation process, q_{cond} is the energy

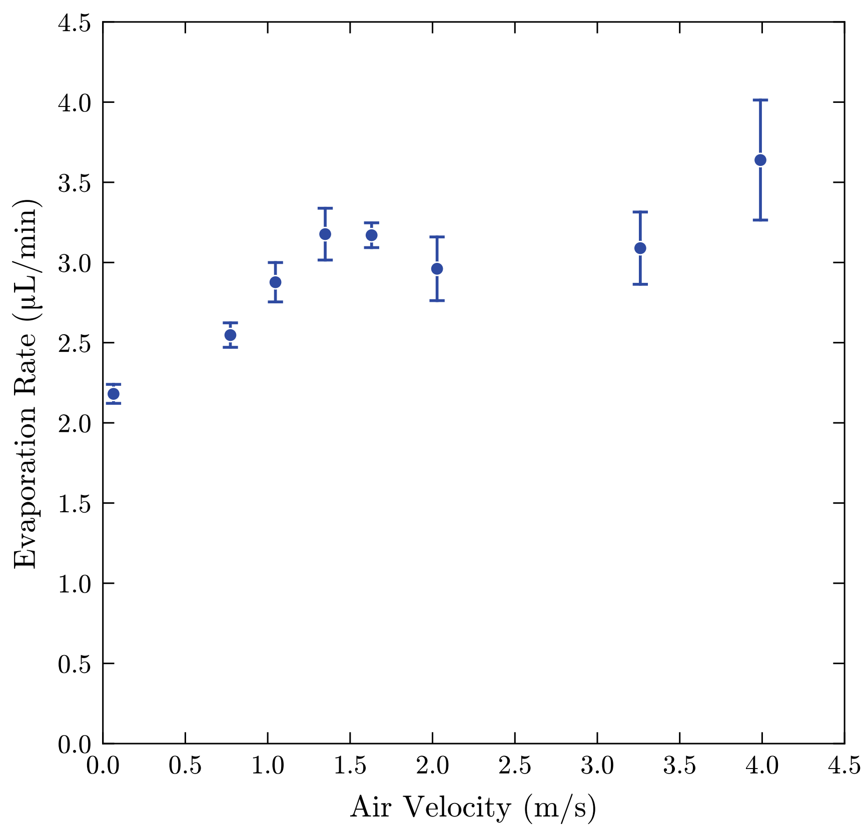

Figure 14: Evaporation rate measurements for the $R = 1.25$ mm droplet at various air velocities from 0 m/s to 4 m/s. Substrate temperature is 55 °C, and droplet height is 1.25 mm.

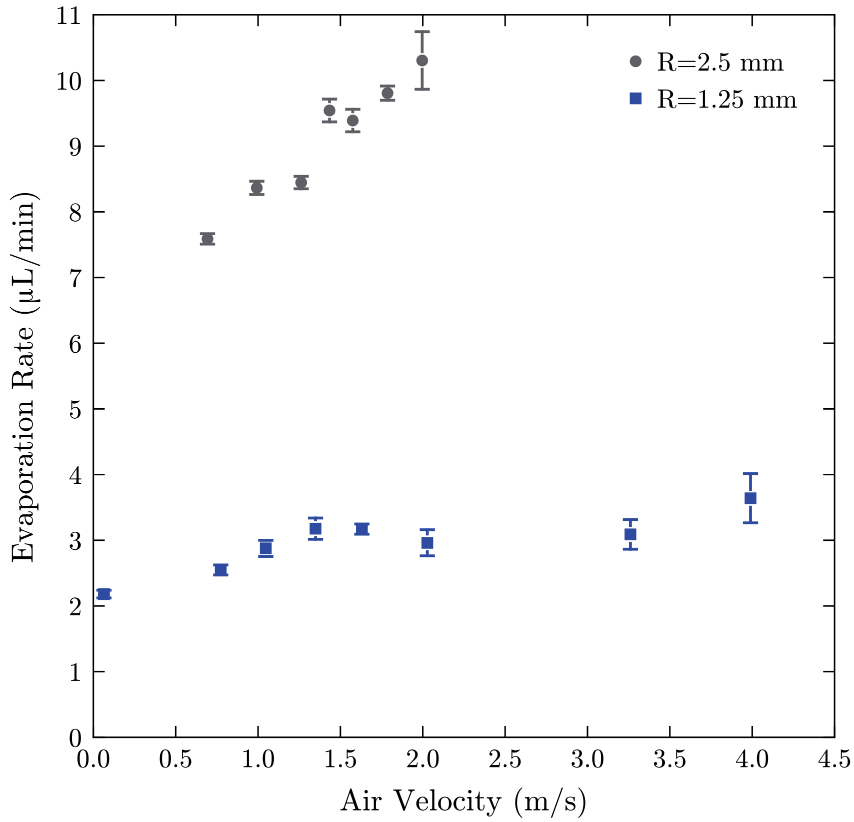

Figure 15: Evaporation rate measurements for both $R = 2.5$ mm and $R = 1.25$ mm droplets.

conduction from the substrate and bulk liquid, $q_{conv,i}$ is the energy transported by convection within the droplet, $q_{conv,e}$ is the energy removed by the convective cooling of the droplet surface by the incoming air flow; a schematic is shown in Figure 16. The enhanced convective cooling at higher air velocities may be a primary factor towards the plateau in evaporation rate increase. At lower air velocities, the effects of removing the vapour-diffusion limit appear to be more significant compared to the rate of energy transport by external convection; but these effects appear to reach a cross-over point when the air velocity reaches ≈2 m/s. In this higher air velocity

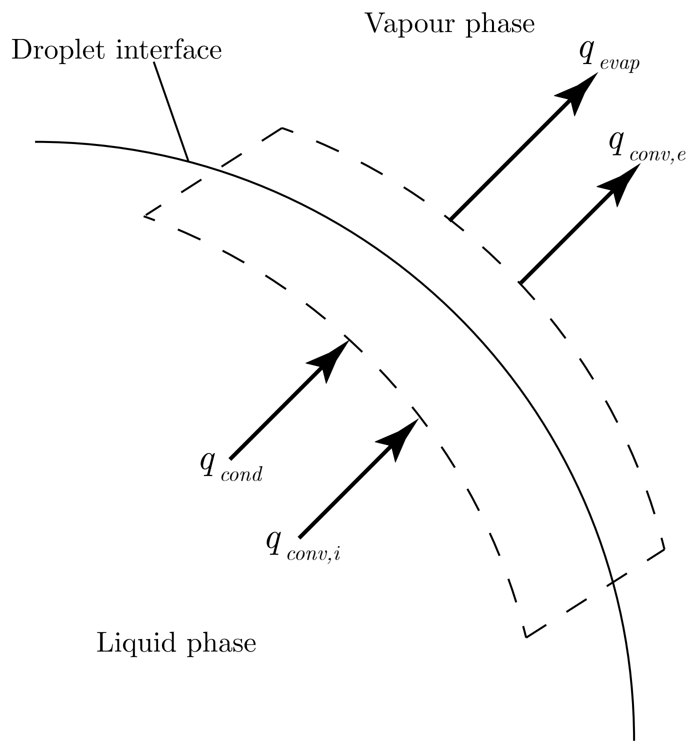

Figure 16: Schematic representation of the energy balance at the droplet interface.

range, the droplet evaporation process appears to be *thermally limited* in the absence of the vapour-diffusion limit. Thus, further experiments are discussed in the following section investigating this potential thermally limited case.

3.2.2 Minimized Temperature Delta

Following the discussion from the previous section, additional experiments were conducted to determine the influence of convective cooling on the evaporation rate. In order to minimize the convective heat transfer caused by the incoming air flow, while ensuring the evaporation process is not vapour-diffusion limited, the ambient air temperature was increased instead. Two experimental cases were investigated, one at an ambient air temperature $T_a = 24°\mathrm{C}$, and a second case at $T_a = 40°\mathrm{C}$. This air temperature corresponds to the upper limit of operating temperatures for the DSLR camera and syringe pump. The substrate temperature was maintained at 40°C to minimize the temperature delta, and thus convective cooling effects. All experiments were tested on the $R = 1.25$ mm droplet, and droplet height was maintained at 1.25 mm for a hemispherical droplet shape. Relative humidity levels were kept at $35 \pm 3\%$ for all cases. The measured evaporation rates for each case are plotted in Figure 17.

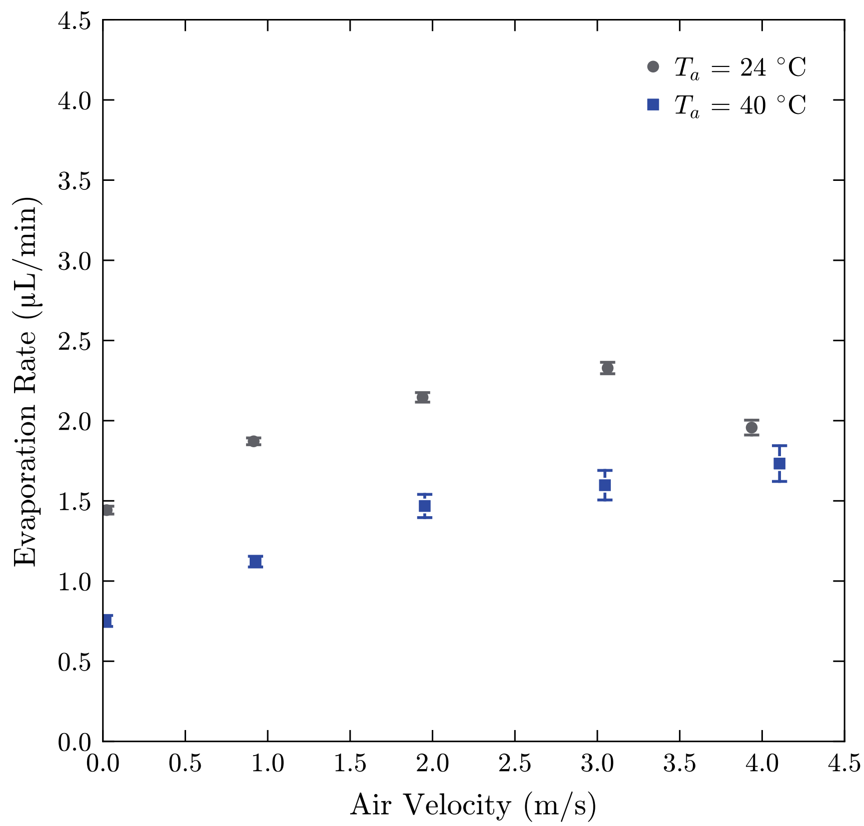

Figure 17: Evaporation rate measurements for the $R = 1.25$ mm droplet under ambient air temperatures of 24 °C and 40 °C. Air velocity was adjusted from 0 to 4 m/s. Substrate temperature was 40 °C and the droplet height was 1.25 mm.

From these results, it is clear that the evaporation rate is reduced when the ambient air temperature is increased. In the air velocity range of 0 m/s to 3.2 m/s, the evaporation rate is consistently reduced by an average of 0.71 ± 0.04 μL/min. This reduction in evaporation rate may be a result of several effects caused by the high ambient air temperature. When the air and substrate temperatures are nearly the same, not only is the external convective cooling reduced, but the internal convection as well. Buoyancy-driven convection and thermocapillary convection are both temperature-dependent mechanisms; in the absence of an imposed temperature gradient between the solid and gas phases, only the evaporative cooling of the droplet interface may produce a temperature delta to initiate these flows. As a result, the velocity magnitude of potential internal flows may be reduced. Simultaneously, the minimized temperature delta will also reduce the rates of energy transport by conduction, $q_{cond} = -k\nabla T$, and convection, $q_{conv} = \bar{h}A\Delta T$ [61]. The influence of these energy transport mechanisms appear to be greater than the influence of increased vapour saturation pressure as a result of the higher air temperature.

Comparison of the measured evaporation rate at an air velocity of 4 m/s suggests that at higher velocities, the evaporation process may be thermally limited. For the $T_a = 24$°C case, the evaporation rate drops by a factor of 0.84, from 2.32 to 1.95 μL/min when the air velocity is increased from 3.2 m/s to 4 m/s. Meanwhile, for the $T_a = 40$°C case, the evaporation rate increases slightly under the same air velocity increase. The reduction experienced at $T_a = 24$°C may be attributed to a similar convective cooling effect observed in the previous case, and compounded by the reduced substrate temperature. Overall, the trend between evaporation rate and air velocity at the elevated air temperature appears to be asymptotic.

3.2.3 Influence From External Droplets

In the preceding sections, discussion has been focused on evaporation of an isolated droplet. However, practical applications utilizing droplet geometries for evaporative cooling will necessitate large droplet arrays to achieve high heat removal rates. The presence of additional droplets may have a significant effect on the evaporation process, even in the absence of external air flows [43]. The fabrication of substrates for continuously-fed droplet arrays has a number of challenges related to the formation of uniform droplets and maintaining constant flow rates [62]; addressing these challenges would require more extensive analysis on the flow behaviour within the substrate and analysis of porous foams and membranes. These considerations are beyond the scope of this work, and therefore emphasis is placed on the influence of additional droplets on the air flow behaviour and whether this may affect the evaporation process, without consideration for the existence of vapour produced by multiple droplets.

In order to test the influence of adjacent droplet geometries, several substrate attachments were designed and 3D printed (Prusa i3 Mk2), shown in Figure 18. Three variations were developed, a flat plate without any droplets, one with a single artificial droplet placed two diameters in front of the actual droplet, and one with two artificial droplets placed two diameters in front, and spaced two diameters apart. These substrate attachments were inserted directly in front and upstream of the droplet pedestal; the left edge is aligned with the centreline of the pedestal, the top is level with the pedestal surface so that the droplet heights of the real and artificial droplets are aligned.

Experiments were conducted for each case at air velocities from 1 m/s to 3 m/s at the same ambient air temperature and relative humidity as previous cases, substrate temperatures were maintained at 40°C. As seen from the results plotted in Figure 19, the evaporation rate is reduced when obstructed by the adjacent droplets. However, the measured evaporation rates between the three substrate attachments are nearly identical within the margin of error, regardless of the existence or placement of artificial droplets. The likely explanation for this effect is the development of a boundary layer caused by the flat plate geometry of the artificial droplet attachments. According to Equation 2.1, the 9.75 mm length of the substrate attachment would produce a developed boundary layer 1.9 mm in height, which is larger than the entire droplet. As a result, this may reintroduce the vapour-diffusion limitation due to the reduced

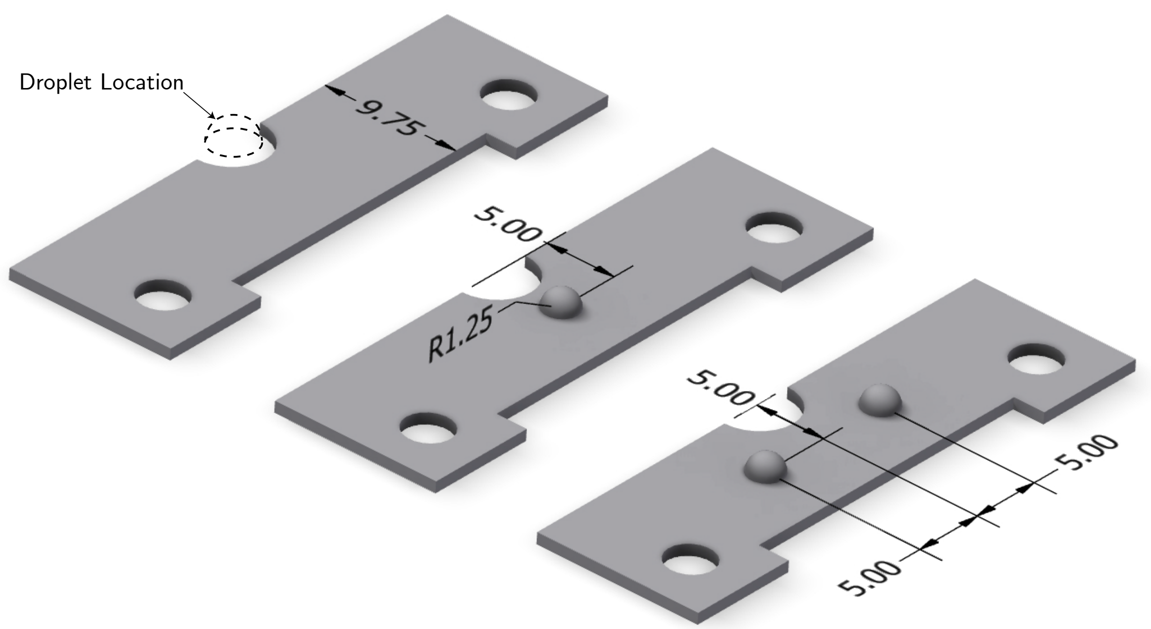

Figure 18: CAD model rendering of the 3D printed substrate attachments. Left: no droplet, middle: single droplet, right: two droplets. Artificial droplets have a radius of 1.25 mm, are spaced four diameters apart. All dimensions above are in millimetres.

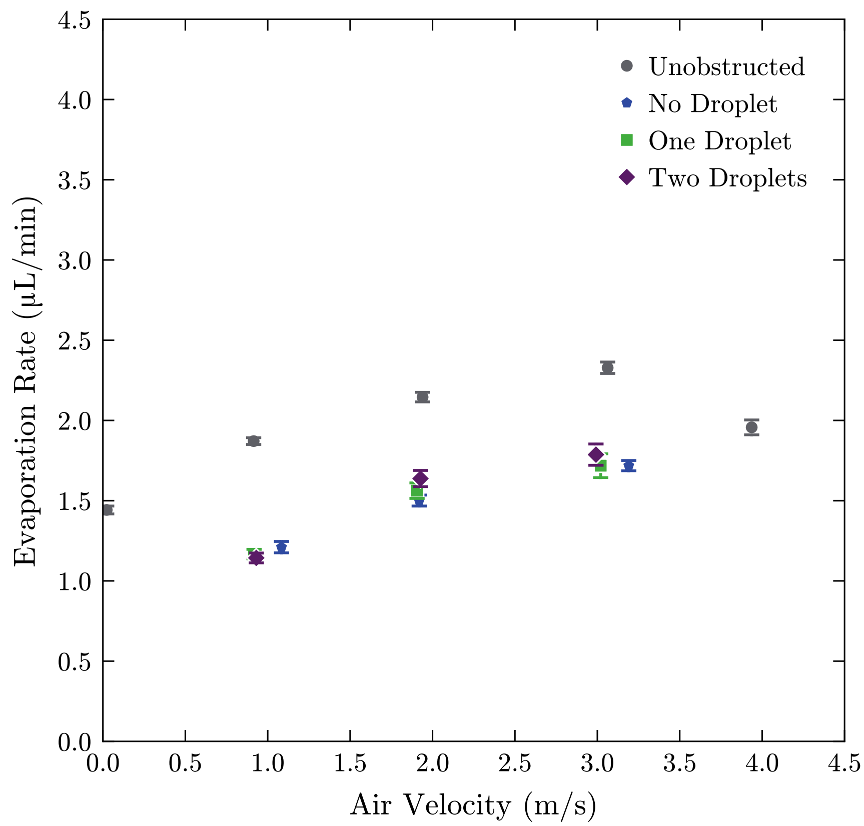

Figure 19: Evaporation rate measurements for the $R = 1.25$ mm droplet at air velocities 1 m/s, 2 m/s and 3 m/s with various substrate attachments to emulate flow effects of adjacent droplets. Substrate temperature was 40°C. Results are compared to the measurements taken for the unobstructed droplet.

mass transport within the boundary layer and therefore reduce the total evaporation rate of the central droplet. This concept of boundary layer development is also consistent with the change in evaporation reduction as air velocity increases. At 1 m/s, the evaporation rate is reduced by a factor of 0.65, while at 3 m/s the evaporation rate in the obstructed cases are only reduced by a factor of 0.74, since the boundary layer height is estimated to be 1.1 mm at the higher air velocity. The evaporation rates while obstructed at 1 m/s are measured to be lower than the rate measured for the unobstructed case at 0 m/s, which at first glance appears unintuitive. This may be explained by considering the effect of vapour transport by natural convection, as discussed by Kelly-Zion et al. [23]. For the unobstructed pedestal geometry, vapour flows outwards and away from the pedestal to avoid saturation at the three-phase contact line. With the presence of the substrate attachment, vapour escaping from the droplet is constrained by the surrounding geometry and may be saturating around the droplet, causing a greater impediment to the evaporation process. These results further suggest the importance of pedestal geometry for maximizing the increases to evaporation rate from forced convection.

Chapter 4

Conclusions

An experimental investigation was conducted to determine the influence of forced convection on the evaporation rate of continuously-fed sessile droplets. To create the necessary conditions for the experiment, a custom experimental apparatus was constructed, which includes a bench-top wind tunnel and a computer-vision based control system. Creating continuously-fed droplets was accomplished using a copper substrate feeding system which constrained the droplet contact line and also allowed accurate control of substrate temperatures. A small scale low-speed wind tunnel was constructed according to recommendations made from literature to generate consistent laminar flows and an environmental chamber was constructed around the entire set up to enable testing at different ambient air temperatures. A computer control system was written in Python to measure droplet heights using computer-vision and automate syringe pump control to determine the droplet evaporation rate.

Five different sets of experiments were conducted with various substrate temperatures and air velocities. The evaporation rates of a 2.5 mm droplet were measured at several substrate temperatures under a constant 1 m/s air velocity; comparing these results with past measurements taken under quiescent conditions showed that evaporation rates increased by a factor of 2.6 at lower substrate temperatures but diminish to a factor of 1.5 at higher substrate temperatures. A second set of experiments with the same droplet radius, but at a fixed substrate temperature and various air velocities between 0.7 m/s and 2 m/s demonstrated a direct linear relationship between evaporation rate and air velocity. The increase of evaporation rate with air velocity was investigated further with a smaller droplet, $R = 1.25$ mm, for air velocities between 0 m/s and 4 m/s. These results showed that the linear increase stops at air velocities above 2 m/s, increasing by smaller increments at 3.25 m/s and 4 m/s; this suggests that energy transport by external convection may become significant at these velocities and the evaporation process becomes thermally limited. Further experimental results compared the evaporation rates at air temperatures of 24°C and 40°C, while the substrate was maintained at 40 °C to minimize the temperature gradient. These results showed that in the absence of an imposed temperature delta, the evaporation rates were reduced by an average 0.71 ± 0.04 μL/min, possibly due to the suppression of internal buoyancy-driven or thermocapillary flows. A final set of experiments investigated the influence of adjacent artificially placed droplets on the air flow behaviour. Results revealed the significant influence of boundary layer growth which reduced overall evaporation rates and demonstrates the importance of using pedestal geometry to maximize the gains produced from forced convection. These results show how the evaporation process for a continuously fed droplet may change when exposed to different air flow conditions, which may aid in future design and development of bioinspired simulated perspiration cooling systems.

4.1 Recommendations

The preceding work was not exhaustive and presents a number of potential questions to be addressed. The following recommendations are beyond the scope of this thesis, but will further the understanding of this evaporation process:

- To investigate the presence of convective cooling and thermal limitation, the droplet interface temperatures can to be measured while evaporating under forced convection. A non-invasive technique such as infrared thermography can provide temperature measurements over the droplet interface.

- The existence and influence of internal convective flows remain unknown, further work involving the use of particle-image-velocimetry may elucidate the mechanisms for these flows. Moreover, the presence of forced convection may overcome buoyancy-driven or thermocapillary effects and determination of how this behaviour changes with air velocity would be valuable to developing a comprehensive model.

- A fully-coupled simulation involving the mass and energy transport phenomena should be developed to model the system. The combination of additional experimental data and high-fidelity simulations can aid in the development of a full analytical model to predict evaporation behaviour outside of vapor-diffusion limited cases.

- A continuously-fed droplet array system is representative of practical cooling applications. Challenges in achieving uniform droplets would need to be addressed. Furthermore, the influence of vapour produced by adjacent droplets within arrays can be investigated to explore the viability of this type of cooling system.

Bibliography

[1] O. Hoegh-Guldberg, D. Jacob, M. Taylor, M. Bindi, S. Brown, I. Camilloni, A. Diedhiou, R. Djalante, K. Ebi, F. Engelbrecht, J. Guiot, Y. Hijioka, S. Mehrotra, A. Payne, S. Seneviratne, A. Thomas, R. Warren, and G. Zhou. Impacts of 1.5°C global warming on natural and human systems, 2018.

[2] H. Bruus. *Theoretical microfluidics*. Oxford university press Oxford, 2008.

[3] R. G. Larson. Transport and deposition patterns in drying sessile droplets. *AIChE Journal*, 60(5):1538–1571, 2014.

[4] Y. A. Cengel and M. A. Boles. *Thermodynamics: an engineering approach*, volume 1000. 2002.

[5] C. Lee and C. R. Wilke. Measurements of vapor diffusion coefficient. *Industrial & Engineering Chemistry*, 46(11):2381–2387, 1954.

[6] V. P. Carey. *Liquid vapor phase change phenomena: an introduction to the thermophysics of vaporization and condensation processes in heat transfer equipment*. CRC Press, 2018.

[7] R. Picknett and R. Bexon. The evaporation of sessile or pendant drops in still air. *Journal of Colloid and Interface Science*, 61(2):336–350, 1977.

[8] K. Birdi, D. Vu, and A. Winter. A study of the evaporation rates of small water drops placed on a solid surface. *The Journal of physical chemistry*, 93(9):3702–3703, 1989.

[9] S. M. Rowan, M. Newton, and G. McHale. Evaporation of microdroplets and the wetting of solid surfaces. *The Journal of Physical Chemistry*, 99(35):13268–13271, 1995.

[10] C. Bourges-Monnier and M. Shanahan. Influence of evaporation on contact angle. *Langmuir*, 11(7):2820–2829, 1995.

[11] H. Hu and R. G. Larson. Evaporation of a sessile droplet on a substrate. *The Journal of Physical Chemistry B*, 106(6):1334–1344, 2002.

[12] H. Hu and R. G. Larson. Analysis of the effects of marangoni stresses on the microflow in an evaporating sessile droplet. *Langmuir*, 21(9):3972–3980, 2005.

[13] H. Hu and R. G. Larson. Marangoni effect reverses coffee-ring depositions. *The Journal of Physical Chemistry B*, 110(14):7090–7094, 2006.

[14] E. F. Crafton and W. Black. Heat transfer and evaporation rates of small liquid droplets on heated horizontal surfaces. *International Journal of Heat and Mass Transfer*, 47(6-7):1187–1200, 2004.

[15] R. Mollaret, K. Sefiane, J. Christy, and D. Veyret. Experimental and numerical investigation of the evaporation into air of a drop on a heated surface. *Chemical Engineering Research and Design*, 82(4):471–480, 2004.

[16] W. Ristenpart, P. Kim, C. Domingues, J. Wan, and H. Stone. Influence of substrate conductivity on circulation reversal in evaporating drops. *Physical Review Letters*, 99(23):234502, 2007.

[17] S. David, K. Sefiane, and L. Tadrist. Experimental investigation of the effect of thermal properties of the substrate in the wetting and evaporation of sessile drops. *Colloids and Surfaces A: Physicochemical and Engineering Aspects*, 298(1-2):108–114, 2007.

[18] G. Dunn, S. Wilson, B. Duffy, S. David, and K. Sefiane. The strong influence of substrate conductivity on droplet evaporation. *Journal of Fluid Mechanics*, 623:329–351, 2009.

[19] F. Girard, M. Antoni, and K. Sefiane. Infrared thermography investigation of an evaporating sessile water droplet on heated substrates. *Langmuir*, 26(7):4576–4580, 2010.

[20] D. Brutin, B. Sobac, F. Rigollet, and C. Le Niliot. Infrared visualization of thermal motion inside a sessile drop deposited onto a heated surface. *Experimental thermal and fluid science*, 35(3):521–530, 2011.

[21] K. Sefiane, J. Moffat, O. Matar, and R. Craster. Self-excited hydrothermal waves in evaporating sessile drops. *Applied Physics Letters*, 93(7):074103, 2008.

[22] B. Sobac and D. Brutin. Thermal effects of the substrate on water droplet evaporation. *Physical Review E*, 86(2):021602, 2012.

[23] P. L. Kelly-Zion, C. J. Pursell, R. S. Booth, and A. N. VanTilburg. Evaporation rates of pure hydrocarbon liquids under the influences of natural convection and diffusion. *International Journal of Heat and Mass Transfer*, 52(13-14):3305–3313, 2009.

[24] P. Kelly-Zion, C. Pursell, S. Vaidya, and J. Batra. Evaporation of sessile drops under combined diffusion and natural convection. *Colloids and Surfaces A: Physicochemical and Engineering Aspects*, 381(1-3):31–36, 2011.

[25] K. Sefiane, S. Wilson, S. David, G. Dunn, and B. Duffy. On the effect of the atmosphere on the evaporation of sessile droplets of water. *Physics of fluids*, 21(6):062101, 2009.

[26] F. Carle, B. Sobac, and D. Brutin. Experimental evidence of the atmospheric convective transport contribution to sessile droplet evaporation. *Applied Physics Letters*, 102(6):061603, 2013.

[27] F. Carle, S. Semenov, M. Medale, and D. Brutin. Contribution of convective transport to evaporation of sessile droplets: empirical model. *International Journal of Thermal Sciences*, 101:35–47, 2016.

[28] S. Y. Misyura. Evaporation of a sessile water drop and a drop of aqueous salt solution. *Scientific reports*, 7(1):14759, 2017.

[29] G. Fang and C. Ward. Temperature measured close to the interface of an evaporating liquid. *Physical Review E*, 59(1):417, 1999.

[30] C. Ward and D. Stanga. Interfacial conditions during evaporation or condensation of water. *Physical Review E*, 64(5):051509, 2001.

[31] H. Ghasemi and C. Ward. Energy transport by thermocapillary convection during sessile-water-droplet evaporation. *Physical review letters*, 105(13):136102, 2010.

[32] K. Gleason and S. A. Putnam. Microdroplet evaporation with a forced pinned contact line. *Langmuir*, 30(34):10548–10555, 2014.

[33] K. Gleason, H. Voota, and S. A. Putnam. Steady-state droplet evaporation: Contact angle influence on the evaporation efficiency. *International Journal of Heat and Mass Transfer*, 101:418–426, 2016.

[34] M. A. Mahmud and B. D. MacDonald. Experimental investigation of interfacial energy transport in an evaporating sessile droplet for evaporative cooling applications. *Physical Review E*, 95(1):012609, 2017.

[35] X. Zhong and F. Duan. Stable hydrothermal waves at steady state evaporating droplet surface. *Scientific reports*, 7(1):16219, 2017.

[36] S. Ye, C.-M. Wu, L. Zhang, Y.-R. Li, and Q.-S. Liu. Evolution of thermal patterns during steady state evaporation of sessile droplets. *Experimental Thermal and Fluid Science*, 98:712–718, 2018.

[37] H. Navaz, E. Chan, and B. Markicevic. Convective evaporation model of sessile droplets in a turbulent flow—comparison with wind tunnel data. *International Journal of Thermal Sciences*, 47(8):963–971, 2008.

[38] L. Bin, R. Bennacer, and A. Bouvet. Evaporation of methanol droplet on the teflon surface under different air velocities. *Applied Thermal Engineering*, 31(17-18):3792–3798, 2011.

[39] E. Isachenko, E. Orlik, and O. Kabov. The effect of the substrate temperature and the height of the mini-channel on the evaporation of liquid droplet blown by the gas flow. In *MATEC Web of Conferences*, volume 72, page 01038. EDP Sciences, 2016.

[40] L. Lecoq, D. Flick, and O. Laguerre. Study of the water evaporation rate on stainless steel plate in controlled conditions. *International Journal of Thermal Sciences*, 111:450–462, 2017.

[41] C. Doursat, L. Lecoq, O. Laguerre, and D. Flick. Droplet evaporation on a solid surface exposed to forced convection: Experiments, simulation and dimensional analysis. *International Journal of Heat and Mass Transfer*, 113:1234–1245, 2017.

[42] N. Shahidzadeh-Bonn, S. Rafai, A. Azouni, and D. Bonn. Evaporating droplets. *Journal of Fluid Mechanics*, 549:307–313, 2006.

[43] O. Carrier, N. Shahidzadeh-Bonn, R. Zargar, M. Aytouna, M. Habibi, J. Eggers, and D. Bonn. Evaporation of water: evaporation rate and collective effects. *Journal of Fluid Mechanics*, 798:774–786, 2016.

[44] W. Ranz, W. R. Marshall, et al. Evaporation from drops. *Chem. eng. prog*, 48(3):141–146, 1952.

[45] W. A. Sirignano. Fuel droplet vaporization and spray combustion theory. *Progress in Energy and Combustion Science*, 9(4):291–322, 1983.

[46] B. Abramzon and W. Sirignano. Droplet vaporization model for spray combustion calculations. *International journal of heat and mass transfer*, 32(9):1605–1618, 1989.

[47] H. Nomura, Y. Ujiie, H. J. Rath, J. Sato, and M. Kono. Experimental study on high-pressure droplet evaporation using microgravity conditions. In *Symposium (International) on Combustion*, volume 26, pages 1267–1273. Elsevier, 1996.

[48] S. S. Sazhin. Advanced models of fuel droplet heating and evaporation. *Progress in energy and combustion science*, 32(2):162–214, 2006.

[49] Y. Zeng and C.-F. Lee. A model for multicomponent spray vaporization in a high-pressure and high-temperature environment. *Journal of Engineering for Gas Turbines and Power*, 124(3):717–724, 2002.

[50] H. Ghassemi, S. W. Baek, and Q. S. Khan. Experimental study on binary droplet evaporation at elevated pressures and temperatures. *Combustion Science and Technology*, 178(6):1031–1053, 2006.

[51] R. S. Volkov, G. V. Kuznetsov, and P. A. Strizhak. Evaporation of two liquid droplets moving sequentially through high-temperature combustion products. *Thermophysics and Aeromechanics*, 21(2):255–258, 2014.

[52] R. S. Volkov, G. V. Kuznetsov, and P. A. Strizhak. Influence of droplet concentration on evaporation in a high-temperature gas. *International Journal of Heat and Mass Transfer*, 96:20–28, 2016.

[53] G. V. Kuznetsov, M. V. Piskunov, and P. A. Strizhak. Evaporation, boiling and explosive breakup of heterogeneous droplet in a high-temperature gas. *International Journal of Heat and Mass Transfer*, 92:360–369, 2016.

[54] P. K. Kundu, I. M. Cohen, and D. Dowling. *Fluid Mechanics*. Elsevier, fourth edition, 2008.

[55] R. D. Mehta and P. Bradshaw. Design rules for small low speed wind tunnels. *The Aeronautical Journal*, 83(827):443–453, 1979.

[56] P. Bradshaw and R. Pankhurst. The design of low-speed wind tunnels. *Progress in Aerospace Sciences*, 5:1–69, 1964.

[57] J. H. Bell and R. D. Mehta. Contraction design for small low-speed wind tunnels. Technical report, NASA, 1988.

[58] T. W. Phillips. pumpy. `https://github.com/tomwphillips/pumpy`, 2015.

[59] S. Suzuki et al. Topological structural analysis of digitized binary images by border following. *Computer vision, graphics, and image processing*, 30(1):32–46, 1985.

[60] ivmech. ivpid. `https://github.com/ivmech/ivPID`, 2015.

[61] T. L. Bergman, A. S. Lavine, F. P. Incropera, and D. P. DeWitt. *Fundamentals of Heat and Mass Transfer, Seventh Edition*. John Wiley and Sons, Inc., 7 edition, 2011.

[62] L. Hou, J. Hagen, X. Wang, I. Papautsky, R. Naik, N. Kelley-Loughnane, and J. Heikenfeld. Artificial microfluidic skin for in vitro perspiration simulation and testing. *Lab on a Chip*, 13(10):1868–1875, 2013.